ÉCOLE DE TECHNOLOGIE SUPÉRIEURE
UNIVERSITÉ DU QUÉBEC

THESIS PRESENTED TO
ÉCOLE DE TECHNOLOGIE SUPÉRIEURE

IN PARTIAL FULFILLMENT OF THE REQUIREMENTS FOR
THE DEGREE OF DOCTOR OF PHILOSOPHY
Ph.D.

BY
Nguyen Duy Phuong TRAN

DEVELOPMENT OF A FLEXIBLE PROTECTIVE SYSTEM
FOR PRESS-BRAKES USING VISION

MONTRÉAL, MARCH 26, 2009

THIS THESIS HAS BEEN EVALUATED

BY THE FOLLOWING BOARD OF EXAMINERS:

Mr. Anh Dung Ngo, Ph.D.,Thesis Supervisor
Department of Mechanical Engineering at École de Technologie Supérieure

Mr. Louis Lamarche, Ph.D., Thesis Co-supervisor
Department of Mechanical Engineering at École de Technologie Supérieure

Mr. Phieu Le-Huy, Ph.D., President of the Board of Examiners
Department of Electrical Engineering at École de Technologie Supérieure

Mrs. Sylvie Nadeau, Ph.D., Examiner
Department of Mechanical Engineering at École de Technologie Supérieure

Mr. Pierre C. Dessureault, Ph.D., External Examiner
Department of Industrial Engineering at Université du Québec à Trois-Rivières

THIS THESIS WAS PRESENTED AND DEFENDED

BEFORE A BOARD OF EXAMINERS AND PUBLIC

FEBUARY 17, 2009

AT ÉCOLE DE TECHNOLOGIE SUPÉRIEURE

ACKNOWLEDGEMENT

DEVELOPPEMENT D'UN SYSTÈME FLEXIBLE DE PROTECTION POUR LES PRESSE-PLIEUSES PAR LA VISION

TRAN, Nguyen Duy Phuong

RÉSUMÉ

Les presse-plieuses sont utilisées dans la plupart des ateliers de fabrication pour le pliage, le formage, le redressage, le poinçonnage et le découpage. Malheureusement, ces machines polyvalentes ont causé de nombreux accidents sur les travailleurs qui devront tenir la pièce ou de mettre les mains dans les zones dangereuses afin de maintenir le rythme de production.

Il est connu que le mouvement du bélier hydraulique dans les presse-plieuses peut être arrêté à tout moment pendant le fonctionnement ce qui est impossible dans le cas des presse-plieuses mécaniques. Pour cette raison, seul le développement d'un système de protection pour presse-plieuse hydraulique est recommandé. Il a également été observé que la plupart des systèmes existants avaient une zone d'interdiction fixe, qui arrête la presse-plieuse hydraulique au moment où les mains du travailleur y entrent. Ces systèmes de protection sont incapables de distinguer le mouvement des mains des travailleurs, qui sont dirigés vers la zone de l'outil de coupe ou vers l'extérieur de cette zone dangereuse. Il est donc trop restreint de répondre aux besoins de production. Afin d'améliorer la flexibilité du système de protection, il est nécessaire de développer un nouveau système. Cette thèse présente le développement d'un système flexible de protection en tenant compte du mouvement de la main du travailleur.

La solution innovante consiste à générer une zone d'interdiction flexible dont les dimensions et la forme dépendent de la vitesse instantanée du point inspecté, du temps d'arrêt de la machine et du temps de calcul du processus. Le mouvement instantané d'un point inspecté sur la main du travailleur est dépisté par des caméras distribuant des différentes vues. La machine sera arrêtée immédiatement chaque fois que le point inspecté est entré dans la zone flexible d'interdiction. L'interférence entre le point inspecté et la zone flexible d'interdiction est déterminée par le vecteur traversable dans l'espace.

Deux approches concernant le nombre de points inspectés sont présentées. Le point inspecté sur la main du travailleur est un point unique et virtuel dans la première approche, tandis qu'au moins trois points virtuels sont dans la deuxième approche. L'objectif de la première approche a pour but de réduire le temps de processus tandis que celui de la deuxième approche a pour but d'augmenter la précision de positionnement des points.

Le travail présenté dans cette thèse prouve que le principe d'établissement de la zone flexible à l'aide de la technologie de vision pour la protection des mains de l'opérateur de presses-plieuses est réalisable.

Mots-Clés: Système flexible de protection, Zone d'interdiction flexible, Presses-plieuses, Vision, Point unique, Multipoints.

DEVELPOMENT OF A FLEXIBLE PROTECTIVE SYSTEM FOR PRESS-BRAKES USING VISION

TRAN, Nguyen Duy Phuong

ABSTRACT

Press-brakes are used in most manufacturing workshops for bending, forming, straightening, punching and trimming. Unfortunately, these versatile machines cause many accidents to workers, who in many cases, must hold the work piece too close to the dies, or must put their hands within the dangerous zones in order to keep up with the rate of production.

It is known that the movement of the ram in hydraulic press-brakes can be stopped instantaneously at any time during the process. For this reason, only a protective system for hydraulic press-brakes is recommended. It has also been observed that most existing systems have a fixed interdiction volume, provoking stoppage of the press-brake whenever the hands of the worker enter this area. These protective systems cannot distinguish motions which are directed towards entering the cutting zone from motions aiming at the exterior of this dangerous zone. They are therefore too restrictive to meet production needs. In order to improve the flexibility of the protective system, it is necessary to develop a new one. This thesis presents the development of a flexible protective system, taking the motion of the worker's hands into account.

The proposed innovative solution consists of generating a flexible interdiction zone, whose dimensions and shape depend on the instantaneous velocity of the inspected point, the machine stopping time, and the calculation time of the processing loop. The instantaneous motion of an inspected point on the worker's hand is tracked using camera sets distributing on the different views. The machine is stopped whenever the inspected point interferes with the flexible interdiction zone. The interference between the inspected point and the flexible interdiction zone is verified using the spatial traversability vector.

Two approaches relating to the number of inspected points are presented. The inspected point on the worker's hand is a single virtual point in the first principle, whereas several virtual points are in the second principle. The first approach deals with the processing time, while the second is aimed at improving the precision.

The work presented in this thesis proves that the principle of the flexible protective zone using vision technology is realizable to protect the worker's hands.

Keywords: Flexible protective system, Flexible interdiction zone, Press-brakes, Vision, Single-point, Multi-point.

TABLE OF CONTENTS

LIST OF TABLES

Page

LIST OF FIGURES

LIST OF ABREVIATIONS

2D	Two dimensions
3D	Three dimensions
ANSI	American national standards institute
CMM	Coordinate measuring machine
OHCI	Open host controller interface
PC	Personal computer

INTRODUCTION

Press-brakes are used in many factories due to their versatility. They can be used to bend, form, straighten pieces, punch holes, and trim edges. However, it has been observed that, during operations, the operator's hands are constantly in the proximity of the hazardous zone [1]. Table 1.1 presents the number of compensated accidents in Québec from 1989 to 1994 reported by the Commission de la Santé et de la Sécurité du Travail du Québec (CSST) [1]. A study published by this governmental agency showed that the percentage of accidents involving the upper limb counted for 35% (approximately 12000 cases) of the total accidents reported during the period of time from 1979 to 1982 [2]. F. Beauchemin and S. Guertin [3] in their study of 184 accidents in five manufactures confirmed that 15% of the accidents were related to press-brakes. Most of the victims were operators (78%), and arms and hands were involved in 67% of the accidents. This evidence shows that the use of press-brakes can be hazardous to the operator's hands.

Table 1.1
Statistics for accidents involving compensation in Québec from 1989 to 1994.
From [1] (1997, pp. 2)

Year	Number of accidents	Death
1989	8947	1
1990	7450	1
1991	6699	5
1992	6031	3
1993	5684	3
1994	4725	1

Much research has been done and many protective systems have been developed in an effort to solve this problem. However, these systems still have limitations concerning the protective zone. Therefore, it is necessary to develop new principles to improve the efficiency of the protective system, for the safety of the machine operator.

Statement of problem

All of the existing protective systems have a fixed protective zone. These systems can't distinguish the motions directed towards entering the cutting zone from the ones aiming towards the exterior area of this dangerous zone. They are therefore too restrictive to meet production needs. In order to improve the flexibility of the protective system it is necessary to develop a new protective system, which can take into account the movement of the worker's hands. In addition, it is known that the movement of the ram in hydraulic press-brake can be stopped instantaneously at any time during the process [1]. For this reason, a new protective system for hydraulic press-brakes is recommended.

Objective and contributions

This work aims at the design of a flexible protective system which is capable taking into account the instantaneous movement of the worker's hands. The research contributions of this thesis are :

- calculation of the kinematic parameters of an inspected point on the worker's hand based on vision;

- proposition of a concept for a flexible interdiction zone based on the instantaneous velocity of the inspected point;

- development of a mean to stop the machine by recognizing the interference between the inspected point and the flexible interdiction zone, calling the spatial traversability vector;

- suggestion of two approaches of protecting the worker's hands, one using single-point inspection and the other using multi-point inspection.

A number of outcomes of this thesis have been published/accepted in the following conferences.
Published:
1.   N.D.P. Tran, A.D. Ngo, and L. Lamarche, 2006. "Development of a Flexible Protective System for Press-Brakes Using Vision - Part I: Algorithm," in *IEEE*

International symposium on industrial electronics. (Montréal, Canada, 9-12 July 2006), vol. 1, pp. 630-634.

2. N.D.P. Tran, A.D. Ngo, L. Lamarche, and Phieu Le-Huy, 2007. "Development of a Flexible Protective System for Press-Brakes Using Vision - Part II: Investigation on the practicability," in *International conference on industrial risk engineering*. (Montréal, Canada, 17-19 December 2007), pp. 396-410.

3. N.D.P. Tran, A.D. Ngo, L. Lamarche, and Phieu Le-Huy, 2009. "Development of a Flexible Protective System for Press-Brakes Using Vision - Part IV: Investigation on the error of the kinematic parameters," in *Proceedings of the Gesellschaft für Arbeitswissenschaft*. (Dortmund, Germany, 3-9 March 2009), pp. 543-546.

Accepted:

4. N.D.P. Tran, A.D. Ngo, L. Lamarche, and Phieu Le-Huy, 2009. "Development of a Flexible Protective System for Press-Brakes Using Vision - Part III: Multi-point inspection," in *International conference on industrial risk engineering*. (Reims, French, 13-15 May 2009).

Organization of the thesis

The thesis consists of three chapters and two appendices. Chapter one gives an overview of the existing protective systems and the related works of localization using vision.

Chapter two presents the first approach of the proposed system, with single-point inspection. This chapter covers the method of calculation of the kinematic parameters of a point on the worker's hand, the concept of the flexible interdiction zone, the spatial traversability vector, and the experimental results.

Chapter three presents the second approach of the proposed system, with multi-point inspection. There is a change in the number and the form of the inspected points, in order to improve precision of the protective system. The algorithm and the experimental results are presented, to validate the improvement.

The conclusion and some suggestions for future improvements are then presented.

The first appendix presents the instantaneous vectors and the corresponding flexible interdiction zones. Finally, the second appendix presents the source code of functions used in the data-flow models.

CHAPTER 1

LITERATURE REVIEW

1.1   The hydraulic press-brake

The operation of a hydraulic press-brake (Figure 1.1) is based on affecting a force on a set of ram and die. This force, which is created by a hydraulic system [4,5], moves the ram to the die in order to bend, form or punch metal. The movement of the ram can be halted at anytime during the process, by setting the status of the solenoids in the hydraulic system.

Figure 1.1   The hydraulic press-brake.
From the website http://www.directindustry.com

1.2   The dangerous zone of the press-brake

The definition of the dangerous zone of the press-brake is described in [1]. The dangerous zone is represented by a three dimensional envelope, whereby two dimensions are the contact surface of the tool and the remaining dimension is the moving distance of the ram (Figure 1.2).
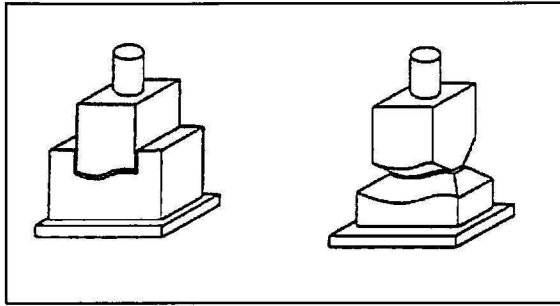
Figure 1.2 The contact surface of the tool.

From [1] (1997, pp. 37)

1.3   The existing protective systems

At present, there are many types of guards available for press-brakes:

Fixed guards: A fixed guard consists of an enclosure for the tools that prevents access of fingers to the trapping area from any direction (Figure 1.3).
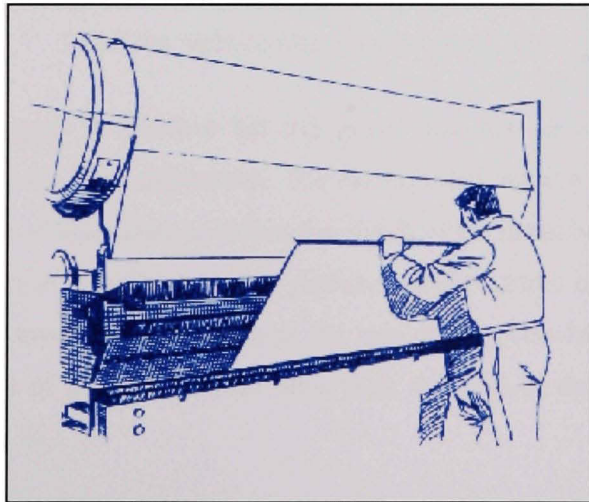
Figure 1.3 Press-brake fixed guard.

From the website http://www.hsbeil.com

Interlocking guards: The interlocking guards consist of a screen across the full width of the bed. This screen is mechanically linked and interlocked with the clutch circuit of the press-brake and has to be down before the press will operate. Once the component material has been loaded into the press brake and trapped by the descending ram, the guard screen rises out of the way (Figure 1.4).
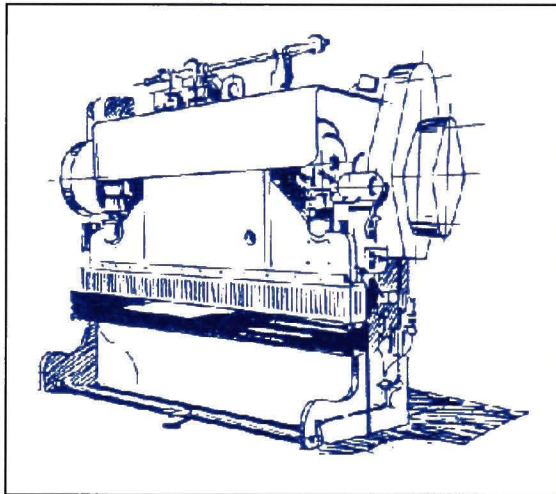
Figure 1.4 Press-brake interlocking guard.
From the website http://www.hsbeil.com

Distance bar trip guard: A distance bar trip guard incorporates a bar, with a screen to prevent access to the tools from underneath. The bar is pulled out to a safe set distance by the operator, and has to be at that distance before the clutch of the press-brakes will operate. This bar is either locked in this position for the duration of the stroke or arranged so that any movement of the bar towards the tools stops the ram of the press-brakes from descending. The sides and the rear of the press-brakes fitted with this type of device are protected with fixed guards (Figure 1.5).

Pullback devices and photo-electric safety devices: Pullback devices utilize a series of cables attached to the operator's hands, wrists, and/or arms. This type of device is primarily used on machines with stroking action. When the slide/ram is in the "up" position, the

operator can feed material, by hand, into the point of operation. When the press cycle is actuated, the operator's hands and arms are automatically withdrawn (Figure 1.6).
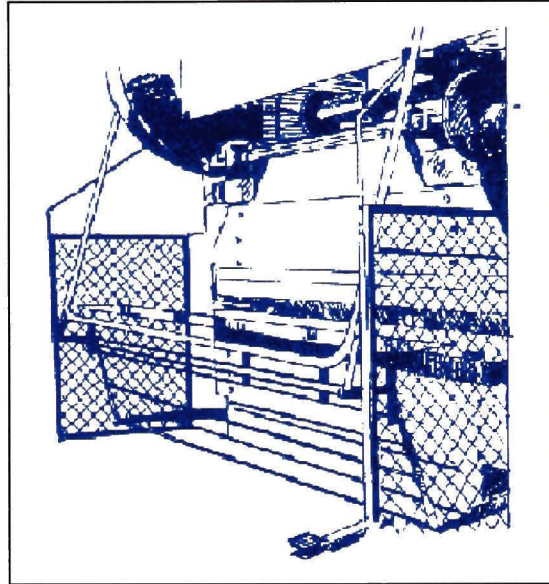
Figure 1.5   Press-brake distance bar trip guard.

From the website http://www.hsbeil.com

NYLON PULLBACK
STRAPS ARE ATTACHED
TO WRISTBANDS
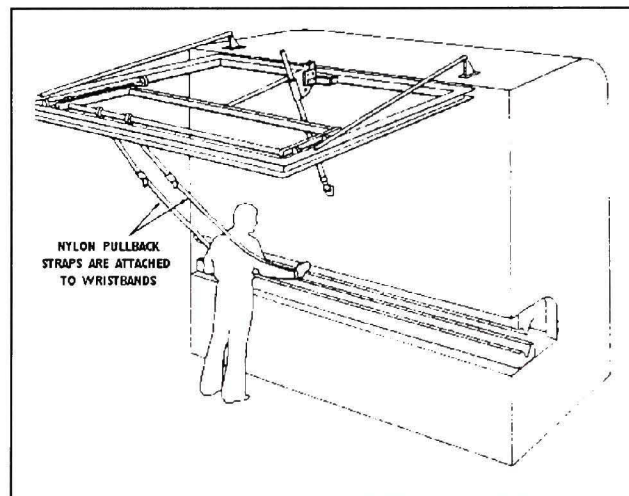
Figure 1.6   Pullback device on press-brake.

From the website http://ehs.uky.edu

A photo-electric guard utilizes a light curtain across the front of the press, which is sensitive to hand or body movement. If this "curtain" of light is broken, it acts as a switch and prevents the operation of the tool (Figure 1.7).
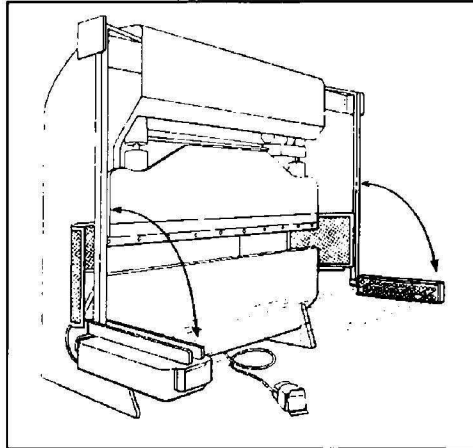
Figure 1.7   Photoelectric presence-sensing device on press-brake.

From the website http://ehs.uky.edu

Laser sensing system: In a laser sensing system, the worker's hands and fingers are protected by a continuous band of red laser light, sensing the zone below the punch [6]. If an obstruction is detected, the movement of the tool is stopped, and then retracted for a small distance (Figure 1.8).
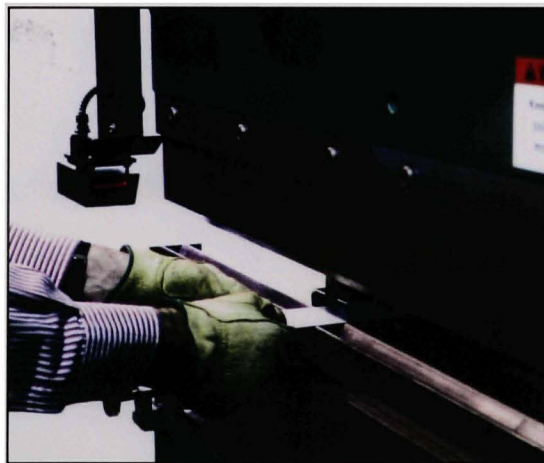
Figure 1.8   Laser sensing system.

From the website http://www.machineguardsolutions.com

Vision-based system: The vision-based system is equipped with a camera that mounts on the punch protecting the worker's hands and fingers during the downward movement of the punch (Figure 1.9). The system creates a safety zone below the punch that is monitored for intrusion. The safety output makes a signal to stop the downward movement of the punch whenever an intruding object is detected [7].

Figure 1.9   Vision-based safety equipment.
From the website http://www.thefabricator.com

1.4   The research of the protective system using vision

C. Kauffman et al. [8] presented a protective method using a vision system. This research was aimed at detecting 2D location of a point of the worker's hand on the image. The solution was based on using a color bracelet on a uniform background in order to extract the bracelet image. By tracking the gravity center of the bracelet, it was possible to recognize the tracking point location on the image. The safety distance was calibrated in the captured image. The machine was stopped whenever the tracking point entered this distance.

J. Velten and A. Kummert [9] also developed a system based on a vision system, which compared the camera image with an image of the empty workspace, having the dangerous

area. The inspection area covering the entire worker's hands was used to extract the endangered components which were hands and fingers. The machine was stopped if the dangerous area was intruded by the endangered components.

1.5   The related works of localization using vision

Ik-Hwan Kim et al. [10] described an active vision system used for object tracking and distance measurement. The authors used a colored ball and the method of look up table, to detect the object in the color image. After the extraction of the ball, the vision system moved the cameras so that the ball's position was at the center of the image. The distance information of the ball was calculated by the trigonometric measurement method.

Jong-Kyu Oh and Chan-Ho Lee [11] presented a stereo vision system for robot guidance. The system included a PC based stereo vision system and a robot system. The interesting point in this research is the investigation of the error when the work-piece is placed at different depths. The experiment showed the change in error following a change of depth. The error which occurred whenever the work-piece was located close to the sides of the image was explained as the effect of lens distortion.

Takushi Sogo et al. [12] described a system for determining location using multiple cameras placed in space, focused in different directions. The results of the paper concentrated mainly on precision. The investigation showed the value of the error whenever the object was placed on some position in 2D space. Moreover, the authors noted that the degree of precision was dependent on various factors such as: the number of sensors, the arrangement of the sensors, and so on.

1.6   Conclusion

Table 1.2 shows the evolution of the protection methods over time. At the beginning, the principle is to prevent the worker's hands entering the dangerous zone. In the next generation, the principle is to detect the obstruction of the worker's hands using the sensor,

which is fixed at a specific distance (the safety distance) from the punch. However, the protective systems presented previously are not able to protect the operator's hands in cases involving the making of small pieces or trays (Figure 1.10).

(a)   (b)
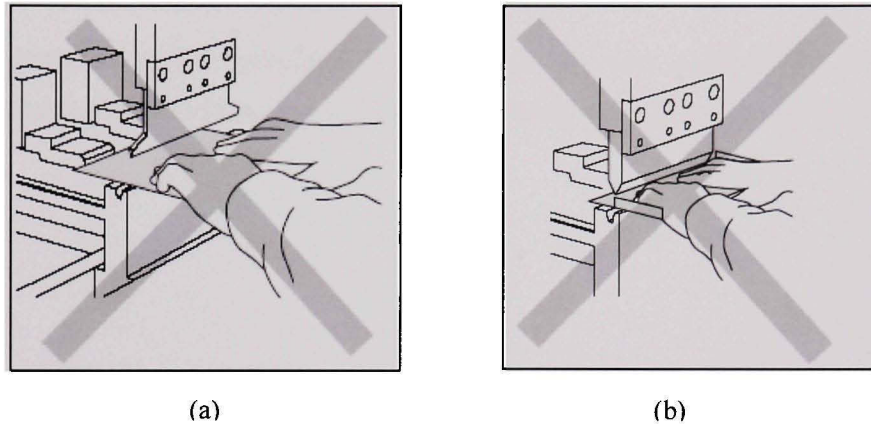
Figure 1.10   Risk of hand injury in cases involving working with small pieces or trays using press-brakes.

(a) making small pieces and (b) making trays.
From [7] (2007, pp. 12)

Table 1.2
The evolution of the protection methods.

Principles	Systems/Researches
Preventing the worker's hands from entering the dangerous zone.	Fixed guards, interlocking guards, distance bar trip guard, pullback devices, and two buttons.
Stopping the machine whenever an obstruction is detected, fixed protective volume.	Light curtain, laser sensing system, and vision based system.
Tracking the worker's hands using vision (2D), fixed protective volume.	C. Kauffman et al. (1996). J. Veltel and A. Kummert (2003).
Tracking the worker's hands using vision (3D), flexible protective volume.	Research work presented in this thesis.

Moreover, the existing systems, including the ones using vision technique, do not consider the direction of the movement of the worker's hands; therefore they are not able to distinguish the dangerous movements from the safe ones. By consequence, they tend to stop the press-brake unnecessarily, and in absence of danger.

The new protective system presented in this thesis has two goals: firstly, tracking the worker's hands using 3D vision; and secondly, generating the flexible protective volume.

CHAPTER 2

THE FLEXIBLE PROTECTIVE SYSTEM WITH SINGLE-POINT INSPECTION

2.1   Principle and definitions

2.1.1   Principle

The operation of the proposed system is based on the flexible interdiction zone. The space in front of the punch is divided into three zones. The first one, which is close to the tool, is called the initial interdiction zone. It is formed without considering the motion of the worker's hand. The next zone is the flexible interdiction zone, in which any intrusion must stop the press-brake. The third zone is the inspection zone, where the kinematic parameters of the worker's hand are determined using two cameras. These parameters are the position and the instantaneous velocity of a given point on the worker's hand. The shape and dimensions of the flexible interdiction zone will be determined using the second parameter in conjunction with the machine stopping time and the calculation time of the processing loop. The stop control system is activated whenever the given point on the worker's hand interferes with the flexible interdiction zone (Figure 2.1).

2.1.2   Definitions

The zones mentioned previously in the principle are defined as follows:

The inspected point is the center of an emitting bracelet worn by the worker during the operation.

The initial interdiction zone, denoted as P_I, is represented by a three-dimensional envelope. Its dimensions depend firstly on the operating space of the punch, secondly on the distance between the inspected point and the tip of the middle finger of the worker's hand, and finally, on the maximum error of the location method (Figure 2.2). This zone is always fixed and independent of the motion of the worker's hand.
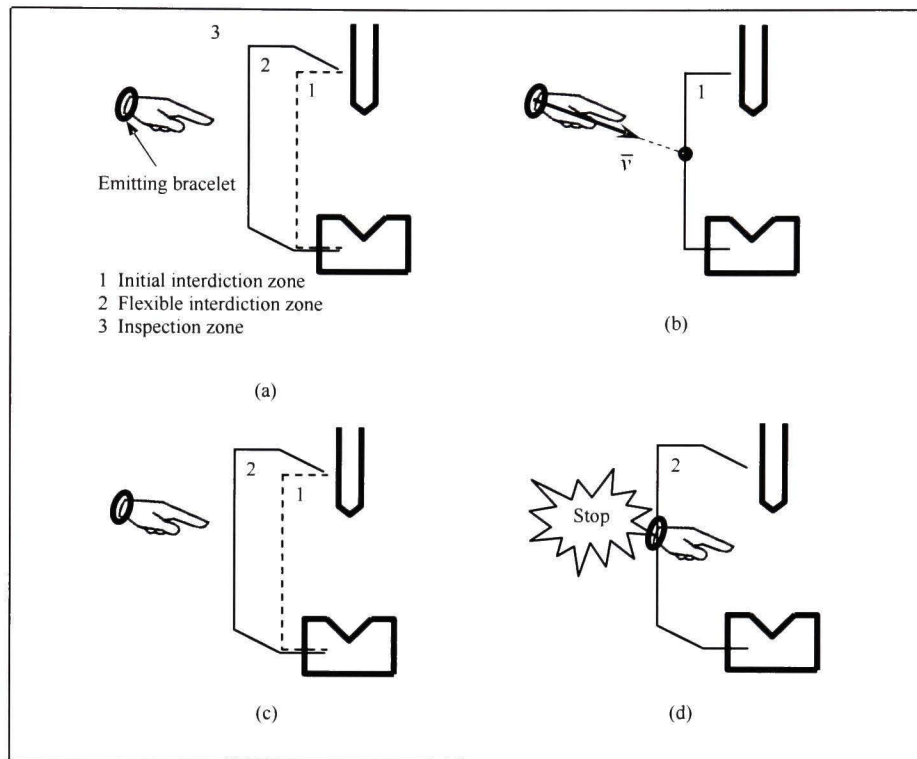
Figure 2.1   The operational principle of the proposed system.

(a) three zones of the flexible protective system.

(b) the condition for the establishment of the flexible interdiction zone.

(c) the instantaneous flexible interdiction zone is generated if the instantaneous velocity intersects with the initial interdiction zone.

(d) the activation of the stop signal depends on the interference between the given point on the worker's hand and the flexible interdiction zone.
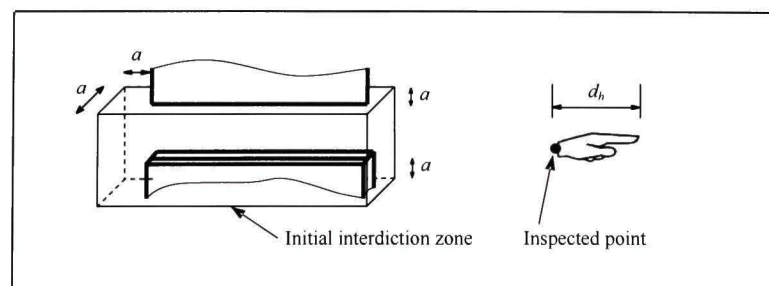
Figure 2.2   Dimensions of the initial interdiction zone.

The dimension "*a*" of the initial interdiction zone illustrated in Figure 2.2 is calculated as follows:

$$a = d_h + d_s + e \qquad (2.1)$$

where

d_h is the distance between the inspected point and the tip of the middle finger.

d_s is an added distance to assure that the tip of the middle finger does not come into contact with the punch. Its proposed value is 10mm.

e is the maximum error of location method.

The inspection zone is the region where the cameras can track the worker's hands.

The flexible interdiction zone, denoted as P_F , is the expanded region of the initial interdiction zone. The shape and dimensions of this zone depend on three elements: the kinematic parameter of the inspected point, the machine stopping time, and the calculation time of the processing loop.

2.2   Algorithm

The global process, whose principle was discussed in the previous section, consists of many successive functional processes, or steps, as presented in the following data-flow model (Figure 2.3).

2.2.1   Multi-view extraction process

The first step is to recognize the image of the emitting bracelet, using the multi-view extraction process. The possibility of the occulted worker's hand is similar for the upper view and the lower view. Therefore, it is necessary to use at least one set of cameras (having two cameras) for each one of these two views. This arrangement guarantees the ability to track the movement of the worker's hand in any operations. Each camera set independently captures and sends the images of the emitting bracelet to its computer. The precision of the

subsequent steps in the global process and the possibility of implementing the system in real-time depend on the performance of the extraction process. For this reason, a filter is used to eliminate the background of the image of the emitting bracelet. Only the image of the bracelet appears on the sensor plane of the camera. In addition, the constant illumination power of the emitting bracelet helps to stabilize the extraction process. Each bracelet must emit an individual color for identification. The extraction process is realized using the color threshold.
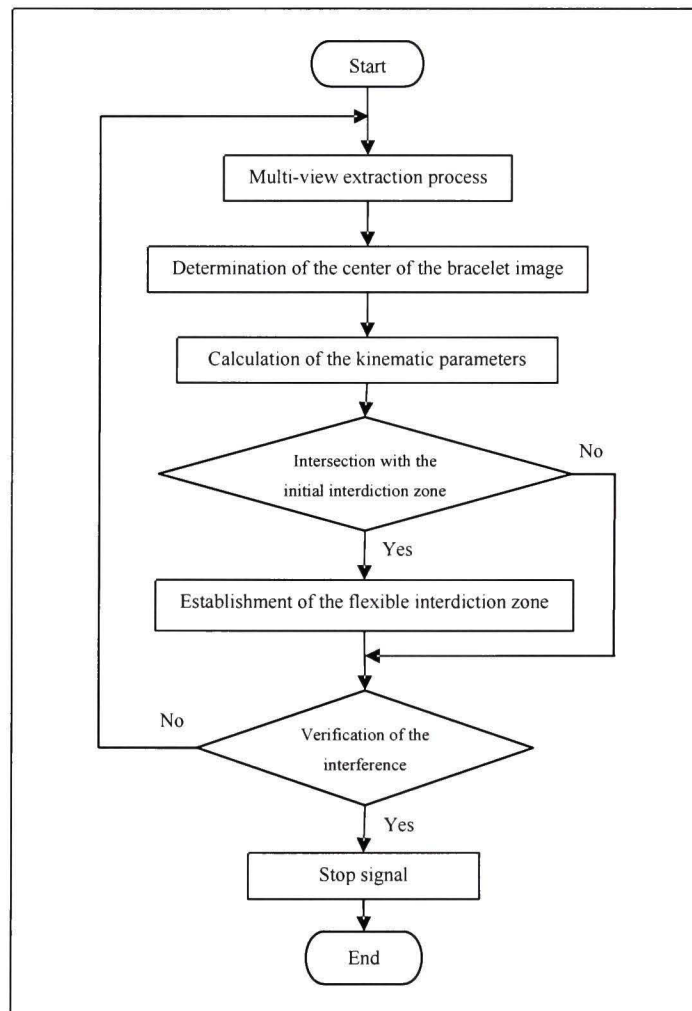
Figure 2.3   Data-flow model of the global process.

Let three matrices I_j ; $j=1,...,3$ be the red, green, and blue elements of the captured image. The threshold T_{jk} needed for extraction of the kth bracelet image of each matrix is chosen by visual observation of the histogram plot and of the specific color of the bracelet. $k=1,...,b$; b is the number of the bracelet. The resulting binary image of each bracelet, denoted as H_k , is determined as follows:

$$H_k = G_1 \, G_2 \, G_3 \qquad (2.2)$$

where

$$G_j[u, v] = \begin{cases} 1 & \text{if } I_j[u, v] \ge T_{jk} \\ 0 & \text{otherwise} \end{cases} \qquad (2.3)$$

u is rows of the matrix.

v is columns of the matrix.

2.2.2   Determination of the center of the bracelet image

On the sensor plane of the camera, the circular bracelet appears as a pixel cloud whose form could be approximated as a line or as an ellipse, depending on the relative positions of the bracelet and the camera. Keeping in mind that the inspected point is the virtual center of the bracelet on the worker's hand, its projection is assumed to be the midpoint of the line or the center of the ellipse.

Firstly, it is necessary to verify the linearity of the pixels having value "one" in the binary image, using a correlation coefficient r:

$$r = \frac{\sum_{i=1}^{n} u_i v_i - n.\overline{u}.\overline{v}}{\sqrt{\left[\sum_{i=1}^{n} u_i^2 - n(\overline{u})^2\right]\left[\sum_{i=1}^{n} v_i^2 - n(\overline{v})^2\right]}}$$

where

r is the correlated coefficient.

u_i , v_i are coordinates of the ith pixel having value "one" pixel in the binary image.

n is the total of pixels having value "one" in the binary image.

$\bar{u}$ is mean of u_i

$\bar{v}$ is mean of v_i

If the absolute value of the correlation coefficient is greater than a predetermined value (in this work this value is 0.98), these pixels form a line. Therefore, the bracelet center is located at the gravity center of these pixels. Otherwise, the image of the bracelet is an ellipse. In the case where the pixel cloud is approximated as an ellipse, the modified version of the A.W. Fitzgibbon [13,14] algorithm is used to approximate the equation of this ellipse. The summary of the problem and the steps of determination of the coefficients of the equation are represented as follows:

Let the implicit equation of the ellipse be presented by following formula:

$$F\left(\bar{a}, \bar{p}\right) = \bar{a} \cdot \bar{p} = au^2 + buv + cv^2 + du + ev + f = 0$$

where

$$\bar{a} = \left[a, b, c, d, e, f\right]^T$$

$$\bar{p} = \left[u^2, uv, v^2, u, v, 1\right]^T$$

$F\left(\bar{a}, \bar{p}_i\right)$ is called the algebraic distance of the ith pixel having coordinates $[u_i, v_i]$ to an ellipse $F\left(\bar{a}, \bar{p}\right)$; $i=1,..,n$

The fitting of this ellipse to the set of the n pixels having value "one" in the binary image is performed by minimizing the sum of the squared algebraic distance of these pixels to the ellipse which is represented by coefficients $\bar{a}$:

$$\min \sum_{i=1}^{n} F\left(\bar{a}, \bar{p}_i\right)^2$$

with the constraint $4ac - b^2 > 0$

The $\bar{a}$ is determined as follows:

$$\bar{a} = \begin{bmatrix} \bar{a}_1 \\ -S_3^{-1}S_2^T\bar{a}_1 \end{bmatrix} \tag{2.4}$$

where

$\bar{a}_1$ is the minimal eigenvector of $M = C_1^{-1}\left(S_1 - S_2S_3^{-1}S_2^T\right)$ which satisfies the condition

$4ac - b^2 > 0$

$$C_1 = \begin{bmatrix} 0 & 0 & 2 \\ 0 & -1 & 0 \\ 2 & 0 & 0 \end{bmatrix} \qquad \begin{aligned} S_1 &= D_1^T D_1 \\ S_2 &= D_1^T D_2 \\ S_3 &= D_2^T D_2 \end{aligned} \qquad D_1 = \begin{bmatrix} u_1^2 & u_1v_1 & v_1^2 \\ \vdots & \vdots & \vdots \\ u_i^2 & u_iv_i & v_i^2 \\ \vdots & \vdots & \vdots \\ u_n^2 & u_nv_n & v_n^2 \end{bmatrix}$$

$$D_2 = \begin{bmatrix} u_1 & v_1 & 1 \\ \vdots & \vdots & \vdots \\ u_i & v_i & 1 \\ \vdots & \vdots & \vdots \\ u_n & v_n & 1 \end{bmatrix}$$

Finally, the coordinates of the ellipse center are calculated using the coefficients of the approximated equation [15]. The coordinates of the ellipse center $[u_{ec}, v_{ec}]$ are calculated using the following formula:

$$\begin{cases} u_{ec} = \dfrac{be - 2cd}{4ac - b^2} \\ v_{ec} = \dfrac{bd - 2ae}{4ac - b^2} \end{cases} \tag{2.5}$$

2.2.3   Calculation of the kinematic parameters

The kinematic parameters, which are the position and the instantaneous velocity of the inspected point, are calculated independently for each view.

2.2.3.1 Determination of the location of the bracelet center

In order to calculate the 3D coordinates of the bracelet center, it is necessary first to determine the camera matrix, then to establish the correspondence of the bracelet image center in the two images appearing in the two cameras.

Determination of the camera matrix: The camera matrix relates the 2D position of a point in the image to its 3D location in space. The direct linear transformation method [16] is used to determine the camera matrices. The summary of the method is as follows:

The camera view and focus are fixed. A calibration object with known coordinates is placed in the scene. The calibration object has n points. The 3D coordinates of the jth point is $\left(x_j, y_j, z_j \right); j=1..n$. The 2D coordinates of the projection of the jth point on the left and the right camera are $\left({}^L u_j, {}^L v_j \right)$ and $\left({}^R u_j, {}^R v_j \right)$. Let ${}^L C$ and ${}^R C$ be the left and the right camera matrix.

Firstly, calculation of the A and B matrix

$$
A = \begin{bmatrix}
x_1 & y_1 & z_1 & 1 & 0 & 0 & 0 & 0 & -x_1{}^L u_1 & -y_1{}^L u_1 & -z_1{}^L u_1 \\
0 & 0 & 0 & 0 & x_1 & y_1 & z_1 & 1 & -x_1{}^L v_1 & -y_1{}^L v_1 & -z_1{}^L v_1 \\
\vdots & \vdots & \vdots & \vdots & \vdots & \vdots & \vdots & \vdots & \vdots & \vdots & \vdots \\
x_j & y_j & z_j & 1 & 0 & 0 & 0 & 0 & -x_j{}^L u_j & -y_j{}^L u_j & -z_j{}^L u_j \\
0 & 0 & 0 & 0 & x_j & y_j & z_j & 1 & -x_j{}^L v_j & -y_j{}^L v_j & -z_j{}^L v_j \\
\vdots & \vdots & \vdots & \vdots & \vdots & \vdots & \vdots & \vdots & \vdots & \vdots & \vdots \\
x_n & y_n & z_n & 1 & 0 & 0 & 0 & 0 & -x_n{}^L u_n & -y_n{}^L u_n & -z_n{}^L u_n \\
0 & 0 & 0 & 0 & x_n & y_n & z_n & 1 & -x_n{}^L v_n & -y_n{}^L v_n & -z_n{}^L v_n
\end{bmatrix}
$$

$$
B = \begin{bmatrix} {}^L u_1 & {}^L v_1 & \cdots & {}^L u_j & {}^L v_j & \cdots & {}^L u_n & {}^L v_n \end{bmatrix}^T
$$

The left camera matrix is determined by this formula:

$$^{L}C = \left(A^{T}A\right)^{-1}A^{T}B \tag{2.6}$$

Performed similarly for the right camera, this will give the necessary two camera matrices.

Determination of the correspondence of the bracelet image center: In order to determine the 3D position of the bracelet center by a vision method, at least two cameras must be used [17]. The key problem then becomes how to establish the correspondence of the bracelet image center appearing in two cameras. The feature-based matching method was adopted for this work. The corresponding feature in this case is the bracelet image center. Keep in mind that in the case of multiple bracelets, the image of each bracelet in two cameras was already identified in the extraction process.

Computation of the 3D coordinates of the bracelet center: It is known that the bracelet center lies on the ray determined by the coordinates of the bracelet image center and the camera matrix. As a result, it must be at the intersection of the lines generated by two cameras. Due to the precision of the approximation and the determination of the camera matrix, the rays might not always intersect. In that case, the midpoint of the connecting segment between the two rays is considered as the inspected point [18].

The requirements for calculation of the 3D coordinates of the bracelet center $\bar{x}_c$ are as follows: Firstly, the cameras matrices ^{L}C and ^{R}C. Secondly, the coordinates of the bracelet image center $\left(^{L}u_{ec}, {}^{L}v_{ec}\right)$ and $\left(^{R}u_{ec}, {}^{R}v_{ec}\right)$.

The two equations to determine the ray passing through the left bracelet image center use the camera matrix ^{L}C and the coordinates of the bracelet image center $\left(^{L}u_{ec}, {}^{L}v_{ec}\right)$:

$$^{L}u_{ec} = \left(^{L}c_{11} - {}^{L}c_{31}{}^{L}u_{ec}\right)x + \left(^{L}c_{12} - {}^{L}c_{32}{}^{L}u_{ec}\right)y + \left(^{L}c_{13} - {}^{L}c_{33}{}^{L}u_{ec}\right)z + {}^{L}c_{14}$$

$$^{L}v_{ec} = \left(^{L}c_{21} - {}^{L}c_{31}{}^{L}v_{ec}\right)x + \left(^{L}c_{22} - {}^{L}c_{32}{}^{L}v_{ec}\right)y + \left(^{L}c_{23} - {}^{L}c_{33}{}^{L}v_{ec}\right)z + {}^{L}c_{24}$$

The remaining ray is determined by using the camera matrix $^R C$ and the coordinates of the bracelet image center $\left(^R u_{ec}, \ ^R v_{ec} \right)$.

Following the method presented in [18], it is necessary to calculate the coordinates of any points P_1 and P_2 on the first ray passing through the left bracelet image center; and the same for points Q_1 and Q_2 on the ray passing through the right bracelet image center (Figure 2.4). After having the coordinates of the needed points, the 3D coordinates of the bracelet center are determined as follows:

$$\bar{x}_c^T = \frac{1}{2} \left\{ P_1 + \left[\frac{\bar{b}\,\bar{u}_1 - \left(\bar{b}\,\bar{u}_2 \right) \left(\bar{u}_1\,\bar{u}_2 \right)}{\left(\bar{u}_1 \right)^2 - \left(\bar{u}_1\,\bar{u}_2 \right)^2} \right] \bar{u}_1 + Q_1 + \left[\frac{\left(\bar{b}\,\bar{u}_1 \right) \left(\bar{u}_1\,\bar{u}_2 \right) - \left(\bar{b}\,\bar{u}_2 \right)}{\left(\bar{u}_2 \right)^2 - \left(\bar{u}_1\,\bar{u}_2 \right)^2} \right] \bar{u}_2 \right\} \quad (2.7)$$

where

$$\bar{b} = Q_1 - P_1$$
$$\bar{u}_1 = P_2 - P_1$$
$$\bar{u}_2 = Q_2 - Q_1$$
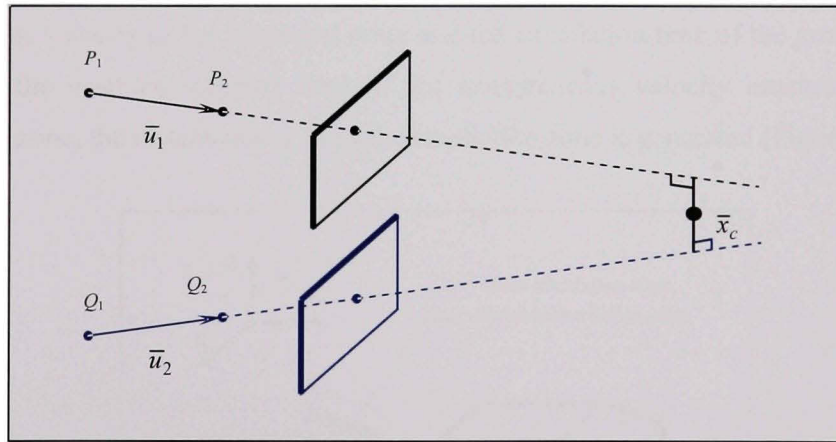
Figure 2.4   Calculation of the 3D coordinates of the bracelet center.

2.2.3.2   Calculation of the instantaneous velocity of the bracelet center

The instantaneous velocity of the inspected point is the second kinematic parameter needed for the establishment of the flexible interdiction zone. This vector is calculated by the following formula:

$$\overline{v}_t = \frac{\overline{x}_t - \overline{x}_{t-\Delta t}}{\Delta t} \tag{2.8}$$

where

$\overline{x}_t$ is the actual position of the inspected point.

$\overline{x}_{t-\Delta t}$ is the previous position of the inspected point.

Δt is the time interval between two captured images.

2.2.4   Establishment of the flexible interdiction zone

The flexible interdiction zone constitutes the principal element of the proposed solution for improving the flexibility of the system.

2.2.4.1   Dimensions of the flexible interdiction zone

The dimensions of the flexible interdiction zone are determined considering the instantaneous velocity of the inspected point and the calculation time of the processing loop, as well as the machine stopping time. If the instantaneous velocity intersects the initial interdiction zone, the instantaneous flexible interdiction zone is generated (Figure 2.5).
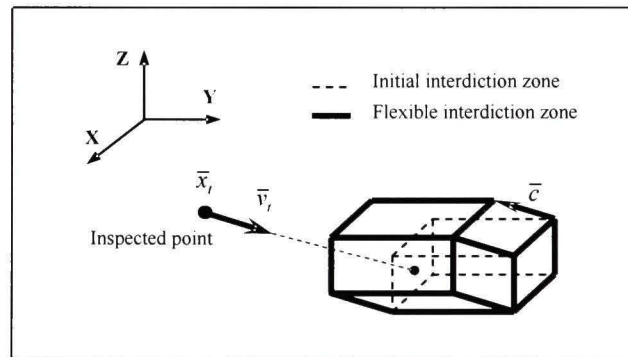
Figure 2.5   Determination of the flexible interdiction zone.

The vector for the dimensional change is calculated as follows:

$$\overline{c} = -k\left(2T_{\text{im}} + T_{\text{sc}}\right)\overline{v}_i \tag{2.9}$$

where

$$\overline{v}_i = \begin{cases} \overline{v}_t & \text{if } \overline{v}_t \text{ intersects with } P_I \\ 0 & \text{ortherwise} \end{cases}$$

$\overline{x}_t$ is the actual position of the inspected point.

$\overline{v}_t$ is the instantaneous velocity of the inspected point.

$\overline{v}_i$ is the instantaneous velocity of the inspected point whenever the condition of the intersection between this vector and the boundary of the initial interdiction zone is satisfied.

k is the safety coefficient.

T_{sc} is the machine stopping time.

T_{im} is the maximum time of the processing loop.

2.2.4.2 Shape of the flexible interdiction zone

The shape of the flexible interdiction zone is determined by considering the interrelation between the direction of instantaneous velocity of the inspected point and the initial interdiction zone. Therefore thirteen possible shapes of the flexible interdiction zone can be generated (Appendix I). In a multi-view system, the flexible interdiction zones are established independently for each view.

2.2.4.3 Example

In this section, a numerical example of establishing the flexible interdiction zone is presented. The data are as follows :

- the punch stroke of the press-brake: 154mm;

- the punch length of the press-brake: 305mm;

- the machine stopping time as presented in an example of ANSI [19] for calculating the safety distance $T_{sc} = 0.18\text{s}$;

- the maximum time of the processing loop of this system $T_{im} = 0.4\text{s}$;

- the distance between the inspected point and the tip of the longest finger $d_h = 160\text{mm}$;

- the add distance $d_s = 10\text{mm}$;

- the maximum error of the location method $e = 20\text{mm}$ (640×480 pixels resolution).

The distance "a" in the initial interdiction zone was calculated using Equation (2.1):

$$a = d_h + d_s + e = 190\text{mm}$$

Figure 2.6 shows the initial interdiction zone with the key points.
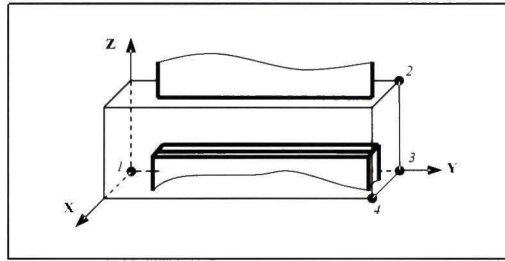
Figure 2.6   The initial interdiction zone.

The coordinates of these points are: $1\,[0, 0, 0]$; $2\,[0, 685, 534]$; $3\,[0, 685, 0]$; $4\,[190, 685, 0]$

Considering an inspected point at $\bar{x}_t = [280, 340, 290]\,\text{mm}$ moving toward the initial interdiction zone with an instantaneous velocity $\bar{v}_t = -[100, 0, 0]\,\text{mm/s}$, the vector for the dimensional change of the initial interdiction zone is:

$\bar{c} = -k\left(2T_{\text{im}} + T_{\text{sc}}\right)\bar{v}_t = 1\left(2 \times 0.4 + 0.18\right)[100, 0, 0] = [98, 0, 0]\,\text{mm}$, with the safety coefficient $k = 1$ (Equation (2.9))

Figure 2.7 shows the shape of the flexible interdiction zone.
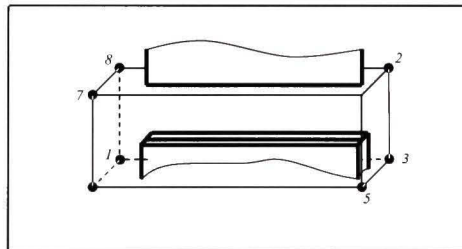
Figure 2.7   The shape of the flexible interdiction zone.

Coordinates of the key points of the flexible interdiction zone are: $1[0,0,0]$; $2[0,685,534]$; $3[0,685,0]$; $5[288,685,0]$; $7[288,0,534]$

2.2.5   Verification of the interference between the inspected point and the flexible interdiction zone

For each view, every moving inspected point establishes a corresponding flexible interdiction zone. The activation of the stop signal depends on the interference between these two elements. This interference is verified using the spatial traversability vector. The first stop signal generated by one of the two views will stop the machine.

2.2.5.1   The spatial traversability vector

The original planar traversability vector was proposed in the literature as a mean to verify the relative position between a point and a convex polygon [20]. In order to verify the relative position between the inspected point and the flexible interdiction zone, which is a convex polyhedron, it is necessary to develop a new mathematical set of equations called spatial traversabilty vector applicable for a 3D case.

Definition of the spatial traversability vector: The spatial traversability vector of a point $\overline{x}$ with respect to the r-sides convex polyhedron is defined as an r-tuple vector:

$$\overline{t}\left(\overline{x},\mathrm{P_F}\right)=[\mathrm{sgn}\left(f_1\right),\mathrm{sgn}\left(f_2\right),\ldots,\mathrm{sgn}\left(f_r\right)] \qquad (2.10)$$

where f_k represents the algebraic distance between the point $\overline{x}$ and the plane k as follows:

$$f_k = \begin{vmatrix} x - x_{1k} & y - y_{1k} & z - z_{1k} \\ x_{2k} - x_{1k} & y_{2k} - y_{1k} & z_{2k} - z_{1k} \\ x_{3k} - x_{1k} & y_{3k} - y_{1k} & z_{3k} - z_{1k} \end{vmatrix} \qquad (2.11)$$

where x_{jk}, y_{jk}, z_{jk} are the coordinates of the jth point (j=1,...,3) creating the kth plane (k=1,..,r) and x, y, z are the coordinates of the point $\overline{x}$.

Determination of the direction of the normal vector of the kth plane: The direction of the normal vector of a plane is determined using the right-hand rule. For example, the positive direction of the normal vector $\bar{n}$ of the plane created by three key points 1, 2, and 3 as shown in Figure 2.8 is, from left to right, derived from the cross product $\bar{n} = (\bar{x}_3 - \bar{x}_2) \times (\bar{x}_1 - \bar{x}_2)$.
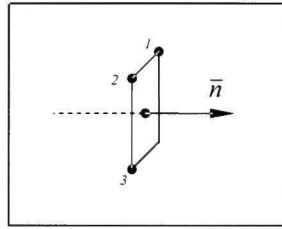
Figure 2.8   The normal vector.

Determination of the algebraic distance f_k between the point $\bar{x}$ and the kth plane: The algebraic value of the distance between the point $\bar{x}$ and the kth plane was determined by the direction of the normal vector of this plane and the position of the point $\bar{x}$ relative to this plane. The algebraic value of this distance is obtained by replacing the coordinates of the point $\bar{x}$ in Equation (2.11). The sgn operator assigns a value of -1, 0, or +1 to the algebraic distance f_k depending on its sign.

Determination of the spatial traversability vector: The spatial traversability vector representing the relative position between a point $\bar{x}$ and a convex polyhedron of r-sides contains r components of sign f_k with k varies from 1 to r. Note that a point $\bar{x}$ located inside the polyhedron generates a known and unique spatial traversability vector.

2.2.5.2   Example

In this example, the r-sides convex polyhedron is the flexible interdiction zone in the example presented in Section 2.2.4.3. The flexible interdiction zone is limited by 6 planes (r=6) (Figure 2.9), from 1 to 6 which were formed by the key points following a

predetermined order: plane 1 (points 8, 1, 6); plane 2 (points 1, 3, 5); plane 3 (points 2, 3, 5); plane 4 (points 7, 8, 2); plane 5 (points 8, 1, 3); plane 6 (points 7, 6, 5). The coordinates of these key points were given previously.
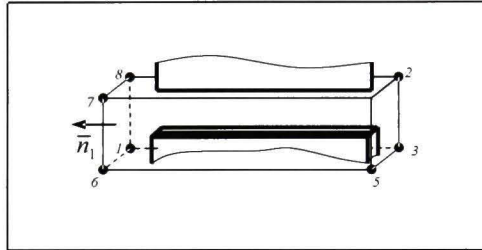
Figure 2.9   The flexible interdiction zone and the normal vector of the plane 1.

Using Equation (2.11), the algebraic distances between an inspected point $\bar{x}_t = [280, 340, 290]$ mm which was located inside of the flexible interdiction zone and the plane 1 of this polyhedron was:

$$f_1 = \begin{vmatrix} x - x_{11} & y - y_{11} & z - z_{11} \\ x_{21} - x_{11} & y_{21} - y_{11} & z_{21} - z_{11} \\ x_{31} - x_{11} & y_{31} - y_{11} & z_{31} - z_{11} \end{vmatrix} = \begin{vmatrix} 280 - 0 & 340 - 0 & 290 - 534 \\ 0 - 0 & 0 - 0 & 0 - 534 \\ 288 - 0 & 0 - 0 & 0 - 534 \end{vmatrix} = -52289280$$

Similarly,

$$f_2 = -57211200 \quad f_3 = 53058240 \quad f_4 = 48136320 \quad f_5 = 102421200 \quad f_6 = -2926320$$

The spatial traversability vector of the inspected point determined by Equation (2.10) was:

$$\bar{t}(\bar{x}_t, P_F) = [-1, -1, 1, 1, 1, -1]$$

Similarly, any point located inside the flexible interdiction zone had the same spatial traversability vector.

2.3   Experimental

2.3.1   Test bench

A test bench was built (Figure 2.10) to simulate the operation of the present algorithm. This test bench includes a press-brake simulator, two mechanical hands, and a flexible protection system based on vision. An aluminium frame whose upper horizontal bar can move up and down was used to simulate the press-brake. The movement of the upper bar was realized by an electric motor and a ball screw. The motor was controlled by a pedal. The punch was attached on the upper bar whereas the die was attached on the lower bar. Two mechanical hands were mounted on two tracks in front of the press-brake. The vision system consists of two digital stereo heads, filters, and emitting bracelets which were fixed on the mechanical hands. The stereo heads were made by Videre Design®. Each of them contained two 6mm focal length lenses. One stereo head was mounted on the upper part of the press-brake whereas the second one was mounted on the lower part of the press-brake. Each stereo head was connected to a computer (Intel® Core 2 Duo 2.66GHz). The welder shade#5 glasses were used as filters. The calculation was executed using a program written in MATLAB®.
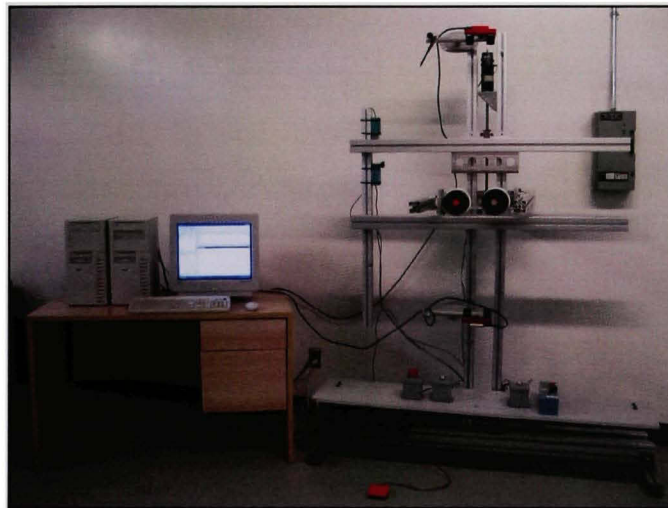
**Figure 2.10   The test bench equipped with a flexible protective system
using multi-view vision.**

2.3.1.1   The emitting bracelet

A circular bulb was used as the emitting bracelet (Figure 2.11). The bulb was fixed on the glove of the worker's hand. The glove was worn by the worker during his operation of the machine. Because the circular bulb was fixed on the glove, the value of d_h in Equation (2.1) is determined by measuring the distance between the center of the circular bulb and the tip of the middle finger of the glove.
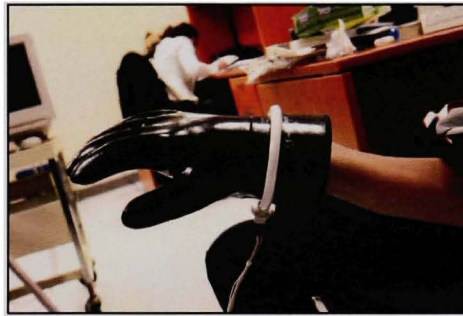
Figure 2.11   The emitting bracelet.

2.3.1.2   The stereo head

The requirement of the system using two cameras to determine the position of a point in space is to acquire and transfer the images of both cameras to the computer simultaneously. Following investigation of existing vision producers, the Videre Design® stereo head was chosen (Figure 2.12). The stereo head has the following characteristics [21] :

- 1280×960 maximum resolution;
- fully synchronized left and right image;
- 1394 interface to standard PC hardware;
- fixed 9cm baseline.

The operation of the stereo head needs the following devices: A computer equipped with 1394 ports (OHCI compliant), a 1394 6-pin to 6-pin cable, and the interface software installed on the computer. Figure 2.13 shows the stereo head which was connected to the

computer. After installing the interface software Small Vision System (SVS), it is possible, using the instruction of "cmat", to set the parameters of the stereo head and to transfer the images to the MATLAB® workspace.
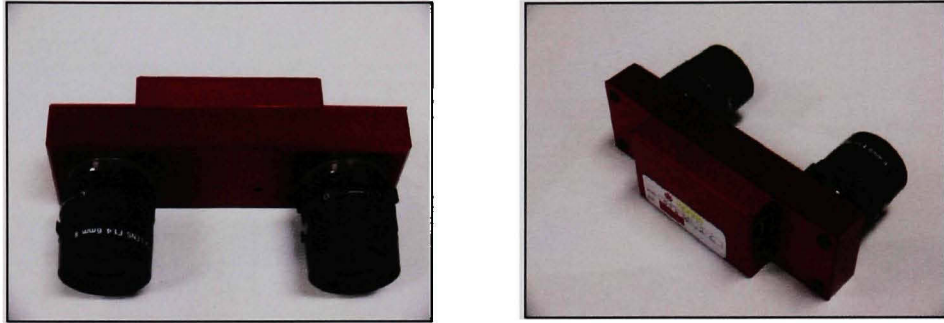
**Figure 2.12   The stereo head.**
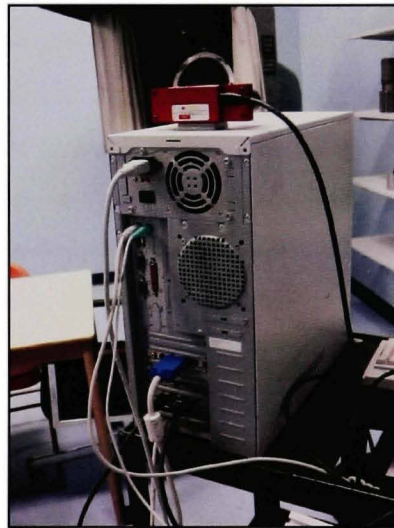
Figure 2.13   Connection of a stereo head with a computer.

2.3.1.3   Image acquisition

A support library was used to interface with MATLAB®. This allows the user to program the whole process in MATLAB®. A testing function was written to determine the time needed to transfer the images from the stereo head to MATLAB® under the various image sizes. Table

2.1 presents the results of the image acquisition time versus the resolution available on the stereo head.

Table 2.1
The average acquisition time.

Size (pixels)	Frame rate (Hz)	The average acquisition time (s)
320×240	30	0.016
640×480	30	0.09
1280×960	7.5	0.43

2.3.1.4   Calibration of the cameras

The cameras were calibrated to determine the two camera matrices of the stereo head. A Mitutoyo Crysta-Apex® coordinate measuring machine was used to measure the 3D coordinates of the marked points on a calibration object (Figure 2.14). The stereo head placed in front of the CMM captured the images of the calibration object. The 3D coordinates of the marked points on the calibration object, measured by the CMM, and the 2D position of these points on the images obtained by the cameras, yield the two camera matrices of the stereo head, as per the method described in Section 2.2.3.1.

2.3.1.5   Processing time

The average time for a global processing cycle per bracelet, without considering the image acquisition time, was 0.2s with 640×480 pixels resolution.

2.3.2   Ability to overcome the occultation problem by using the two-view system

Figure 2.15 shows different occultation possibilities of the inspected point(s) on the worker's hand(s) in a single-view system.
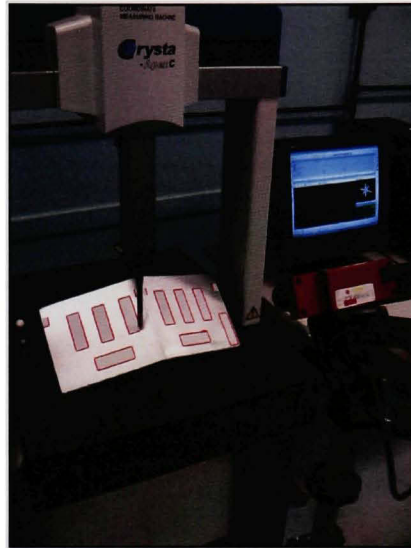
**Figure 2.14 Determination of the coordinates of the marked points
on the calibration object.**

(a)   (b)   (c)   (d)
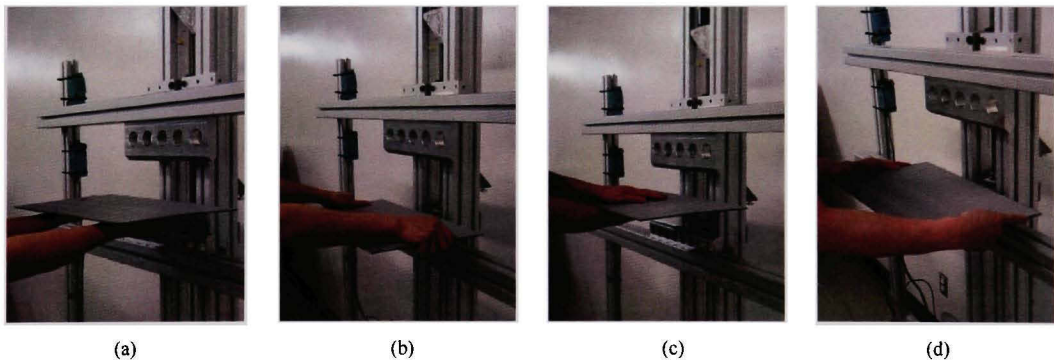
Figure 2.15 Possibilities of occultation of the inspected points.

(a) both of the inspected points are absent in the top view.
(b) both of the inspected points are absent in the bottom view.
(c) one of the inspected points is absent in each view.
(d) the inspected points are wrongly determined by the image of a partly hidden bottom view.

The two-view system which has two sets of cameras placed one at the upper and one at the lower part of the press-brake permits the elimination of the occultation problem. In fact,

when the inspected points enter the inspection zone, they can be tracked by at least one camera set. In the case shown in Figure 2.15a the worker's hands are tracked by the lower set. Figure 2.15b shows the situation where the hands are tracked by the upper set; whereas in the case of Figure 2.15c each camera set tracks one hand. In the case where the bracelets are partly hidden in the bottom view, as shown in Figure 2.15d, the bracelets still appears fully in the upper view. Therefore, the position of the inspected point is determined correctly by the upper view.

2.3.3   The extraction process

The first step of the global process is the extraction of the bracelet from the captured images. The requirement of reducing the processing time and of reliability was met using the emitting bracelet and the filters. Figure 2.16 presents the bracelets and their corresponding binary images after the extraction process.

| (a) | (b) | (c) | (d) |
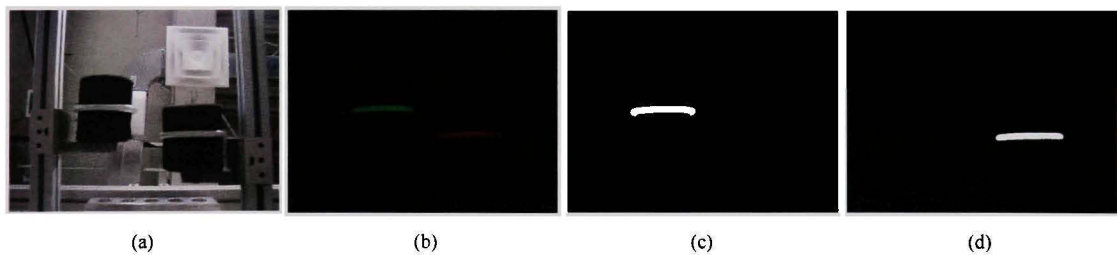
Figure 2.16   The extraction process.

(a) the actual emitting bracelets.
(b) the filtered image of the emitting bracelets.
(c) (d) the corresponding image of the emitting bracelets after the extraction process.

In this figure, the emitting bracelets were placed in the workshop in order to verify the effect of environmental conditions on the method. The result shows that the obtained binary images were found to be independent of environmental conditions. Table 2.2 shows the average time needed for the extraction process in various image resolutions.

Table 2.2

The average time needed for the extraction process in various image resolutions.

Resolution (pixels)	The average time of the extraction process (s)
320 × 240	0.05
640 × 480	0.1
1280 × 960	0.4

2.4   Results

2.4.1   Investigation of the error of positioning

As mentioned in Section 2.2.2, the inspected point is a virtual center of the bracelet. Its location is determined based on the assumption that the projection of the bracelet center is near the ellipse center of the bracelet image. Therefore, it is important to assess the error of this approximation. Figure 2.17 shows the experimental set-up used to compare the coordinates measured directly by the CMM with the results calculated by the vision system.


Figure 2.17   The experimental set-up for the assessment of the error of the present vision method.

A mechanical hand wearing the emitting bracelet was placed on the table of the CMM. The stereo head was placed in front of the CMM. The optical axis of the camera is neither perpendicular, nor parallel to the movement direction of the bracelet. The computer on the left hand side of the CMM, which was connected to the stereo head, calculated the position of the bracelet center by the presented method. The computer on the right side of the CMM displayed the coordinates of the center of the bracelet measured by the CMM. In order to compare the results of the two methods, the machine reference of the CMM was used in all the measurements. The error was evaluated by the difference between the measured position and the calculated position of the bracelet center.

2.4.1.1 Calculation of the bracelet center using the vision system

The first step for the calculation of the coordinates of the bracelet center was to determine the camera matrices. This was described in Section 2.3.1.4. The problem then becomes establishment of the correspondence. As mentioned before, the bracelet image centers were used as the location feature. Therefore it is necessary to determine these points. Figure 2.18 shows the bracelet image center coordinates as calculated.
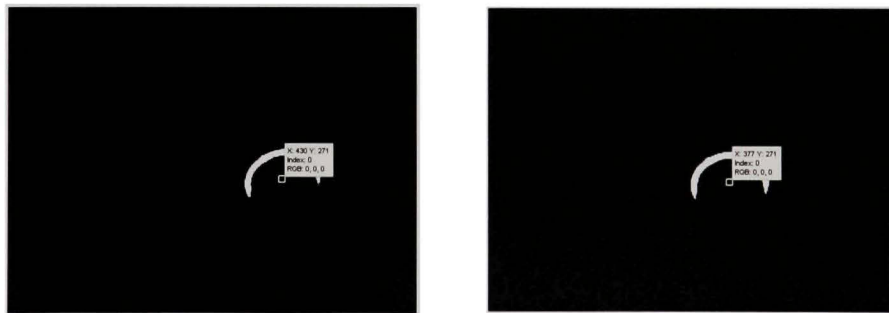

Figure 2.18   The coordinates of the bracelet image centers.

Using the camera matrices and the corresponding bracelet image coordinates; it is possible to determine the coordinates of the bracelet center.

2.4.1.2   Measurement of the bracelet center using coordinate measuring machine

The coordinates of the bracelet center were also determined independently using CMM (Figure 2.19). Because the bracelet is circular in shape, the CMM function for circle measurement was used. The result of the measurement supplies the necessary information, including the coordinates of the center of the circle and the diameter of the circle.

2.4.1.3   The difference between the measured position and the calculated position of the bracelet center

Due to the experimental conditions, it was decided to focus on two factors: firstly the distance between the stereo head and the bracelet, and secondly the image resolution. Table 2.3 illustrates the difference between the coordinates measured by the CMM and the results obtained by the vision system in various distances under two resolutions: 640×480 pixels and 1280×960 pixels.
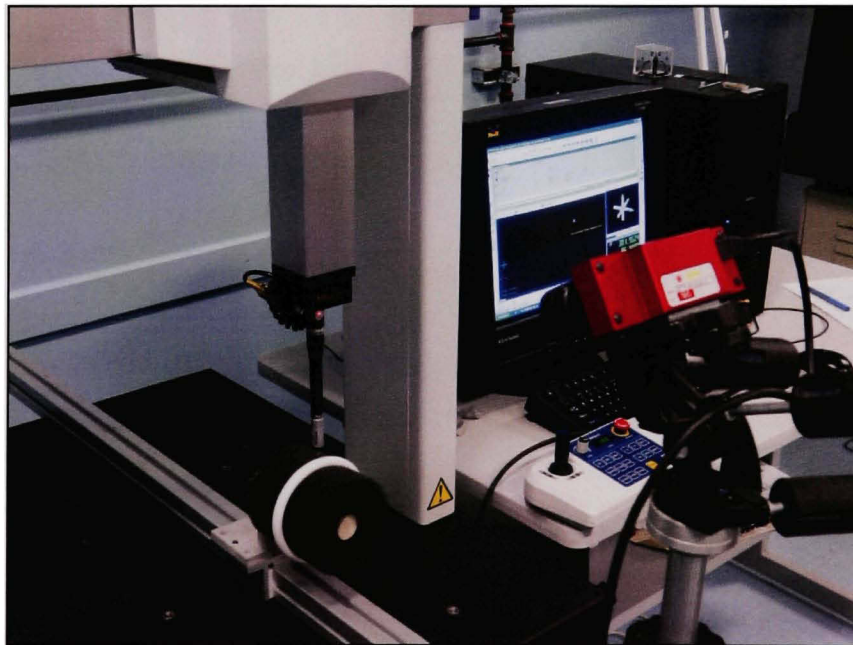

Figure 2.19   Measurement of the bracelet center using CMM.

Table 2.3

The difference between the coordinates measured by the coordinate measuring machine and the results obtained by the vision method in various distances and resolutions.

Distance	Measured by the CMM [x, y, z]* (1)	Resolution 1280×960 [x, y, z]* (2)	Resolution 640×480 [x, y, z]* (3)	Difference** [Δx, Δy, Δz]* (4) = (1) – (2)	Difference** [Δx, Δy, Δz]* (5) = (1) – (3)
~700 mm	[422±0.5, 41±0.5, 166±0.5]	[424±0.3, 48±0.5, 164±0.3]	[427±0.3, 56±0.5, 157±0.3]	[-2, -7, 2]	[-5, -15, 9]
~800 mm	[422±0.5, 182±0.5, 166±0.5]	[423±0.3, 190±0.5, 164±0.3]	[427±0.3, 198±0.5, 157±0.3]	[-1, -8, 2]	[-5, -16, 9]
~900 mm	[422±0.5, 282±0.5, 166±0.5]	[424±0.3, 292±0.5, 163±0.3]	[428±0.3, 300±0.5, 156±0.3]	[-2, -10, 3]	[-6, -18, 10]
~1000 mm	[422±0.5, 377±0.5, 166±0.5]	[424±0.3, 389±0.5, 163±0.3]	[428±0.3, 396±0.5, 156±0.3]	[-2, -12, 3]	[-6, -19, 10]

* in mm

** difference between the mean values

Columns (4) and (5) of Table 2.3 show that firstly, the higher the image resolution, the better the precision and secondly, the farther the distance separating the stereo head and the bracelet in the y direction, the larger the difference between the values of the y coordinate obtained by two measurement methods. It is known that the range resolution of the stereo head (the minimum distance that the stereo head can distinguish) is the main factor related to the precision of the vision system [21]. In order to recognize the movement of the inspected point with greater precision, it is necessary to increase the resolution.

2.4.2 Investigation of the error of magnitude of the velocity vector

The instantaneous velocity vector of the inspected point is one of elements affecting the dimensions of the flexible interdiction zone. Therefore, it is necessary to assess the error of this value. Figure 2.20 shows the experimental set-up permitting to comparison of the magnitude of the velocity vector of the inspected point, created by the motorized linear positioner, with the results calculated by the vision system.

A mechanical hand wearing the emitting bracelet was placed on the table of the motorized linear positioner, which was controlled by the PC on the left hand side of the positioner

(made by Thomson®). The velocity of the bracelet center was thus, equal to the speed of the table. The speed of the table could be set manually by using the software furnished with the positioner. The stereo head was placed in front of the positioner. The computer on the right hand side of the slide, which was connected to the stereo head, calculated the magnitude of the velocity of the bracelet center by using the vision technique. The error was evaluated by the difference between the set velocity value and the calculated velocity value.

According to the results of Section 2.4.1.3, the precision increases when the stereo head works with a high resolution (1280×960 pixels). Unfortunately, the available frame rate is limited with this resolution. Therefore, it was decided to perform the assessment with the 640×480 pixels resolution (30 frames per second).

The difference was found whenever the bracelet was placed at various distances from the stereo head. Table 2.4 illustrates the difference between the velocity set on the linear positioner and the results obtained from the vision system.
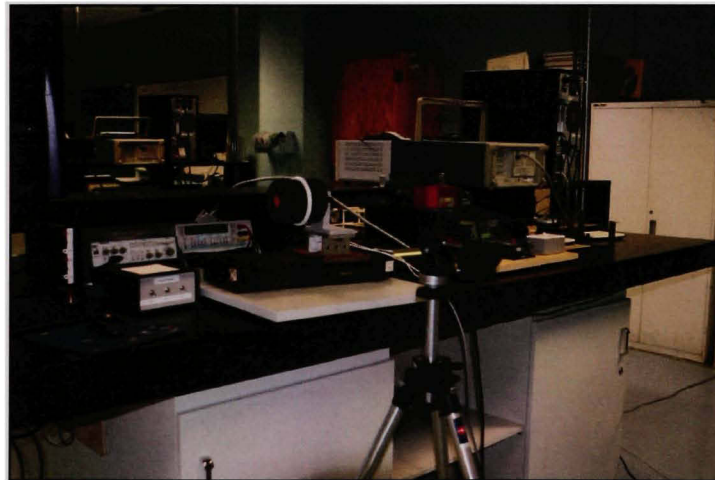
Figure 2.20 The experimental set-up for the assessment the error of the velocity magnitude of the bracelet center.

Table 2.4 shows that the difference between the setting value of the velocity magnitude and the calculated one is proportional to the distance between the stereo head and the bracelet. This error might come from the error of the y coordinate in the process of calculation of position of the bracelet center.

Table 2.4
The difference between the velocity set on the linear positioner and the results obtained by the vision system at various distances with a resolution of 640×480 pixels.

Distance	The velocity magnitude set on the linear positioner (mm/s)	The minimum and the maximum value of the calculated velocity magnitude (mm/s)	The number of measurement
~400 mm	8	7.9 - 8.3	50
~500 mm	8	7.9 - 8.4	50
~700 mm	8	8.4 - 8.8	50
~900 mm	8	8.4 - 9.0	50

2.5   Conclusion

This chapter presents the development of the first approach of a new protective system for press-brakes based on vision with single-point inspection, precisely the center of a bracelet worn by worker's hand. The main feature of this innovative solution is the concept of a flexible interdiction zone. By using two stereo heads, the motion of the worker's hand can be tracked in order to establish the flexible interdiction zone in real-time. The spatial traversability vector for the 3D case was proposed in order to verify the interference between the inspected point and the flexible interdiction zone. Experimental results were stable, proving the reliability of the method.

CHAPTER 3

THE FLEXIBLE PROTECTIVE SYSTEM WITH MULTI-POINT INSPECTION

3.1 Principle and definitions

3.1.1 Principle

The operation of the proposed system is based on the concept of the flexible interdiction zone. The space in front of the punch is divided into three zones: the initial interdiction zone, the flexible interdiction zone and the inspection zone. There is an increase the number of inspected points on the worker's hand. Several inspected points are attached to the worker's hand (Figure 3.1). At any given moment, every inspected point has a corresponding flexible interdiction zone. The stop control system is activated whenever an interference between an inspected point and the corresponding flexible interdiction zone occurs.
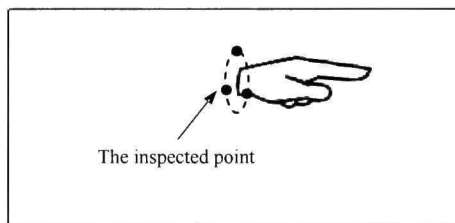

Figure 3.1   The inspected points on the worker's hand.

3.1.2 Definitions

The definitions of the inspected point and the zones relating to the protection system are as follows:

The inspected point is the center of an emitting sphere fixed on the circular hand bracelet worn by the worker during the operation. In order to prevent occultation, the bracelet has to be equipped with at least three emitting spheres. There are thus many inspected points on the

hand bracelet. This is the fundamental difference between this approach and the previous one.

The initial interdiction zone, denoted as P_I, is represented by a three-dimensional envelope. Its dimensions depend firstly on the operating space of the punch, secondly on the distance between the center of the bracelet holding the emitting spheres and the tip of the middle finger of the worker's hand, thirdly on the distance between the center of the bracelet and the center of the sphere and finally, on the maximum error of location method (Figure 3.2). This zone is always fixed and independent of the motion of the worker's hand.
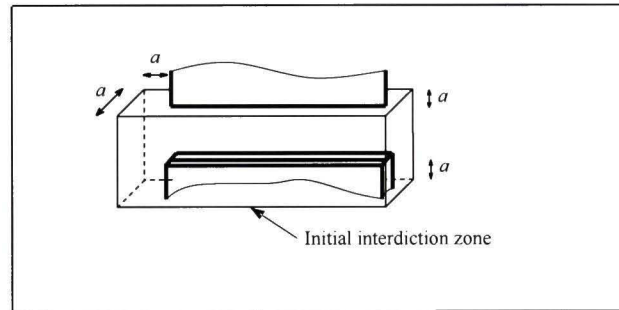

Figure 3.2   Dimensions of the initial interdiction zone.

The dimension "a" of the initial interdiction zone illustrated in Figure 3.2 is calculated as follows:

$$a = d_h + d_s + r + e \tag{3.1}$$

where

d_h is the distance between the center of the bracelet with the attached emitting spheres, and the tip of the middle finger.

d_s is an added distance to assure that the tip of the middle finger does not come into contact with the punch. Its proposed value is 10mm.

r is the distance between the center of the bracelet and the center of the sphere.

e is the maximum error of location method.

It is important to mention here that the dimension "a", which is the minimum safe distance to avoid contact between the tip of the worker's finger and the punch, is equal to the distance between the tip of the middle finger and the center of the emitting sphere, plus the maximum error of the location method "e" and the added distance "d_s". However, the distance between the tip of the middle finger and the center of the emitting sphere varies with the inclination of the bracelet during the operation. Therefore, for the reason of safety, the sum of two fixed distances "d_h" and "r" are proposed, to assure that the distance between the tip of the middle finger and the center of the emitting sphere is always smaller than this value.

The inspection zone is the region where the cameras can track the worker's hands.

The flexible interdiction zone, denoted as P_F, is the expanded region of the initial interdiction zone. The shape and dimensions of this zone depend on three elements: the kinematic parameter of the inspected point, the machine stopping time, and the calculation time of the processing loop.

3.2   Algorithm

The multi-points inspection approach implies some change in the global process. Figure 3.3 shows the new global process.

3.2.1   Multi-view extraction process

The protective system uses at least one set of cameras for the upper view and the lower view. Each camera set independently captures and sends the images of the emitting spheres to its computer. Each sphere must emit an individual color for identification. The extraction process is realized using the color threshold.
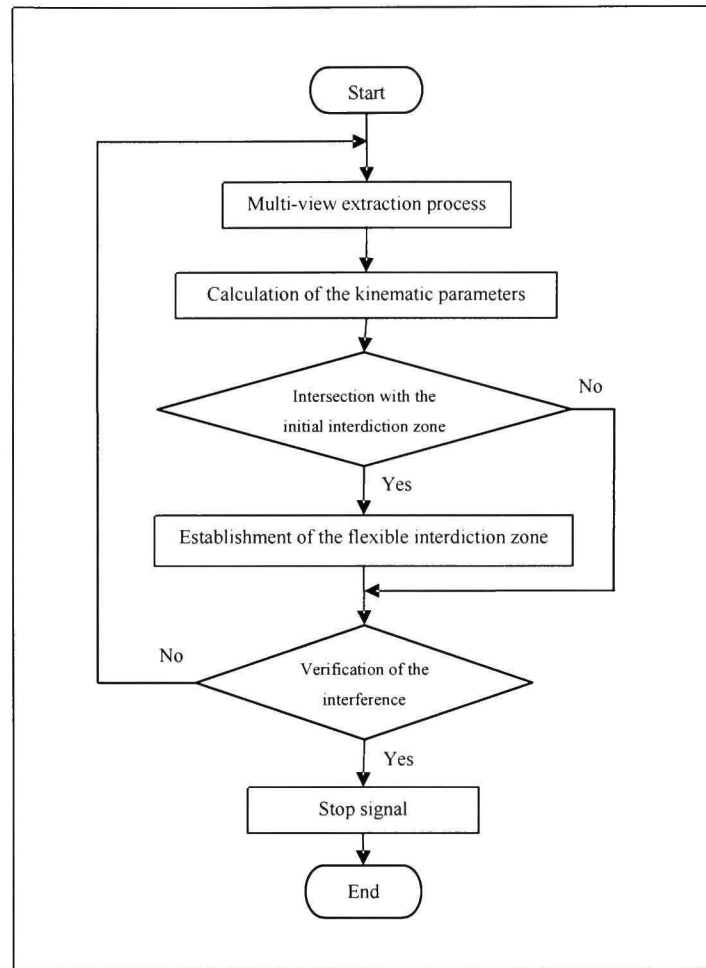
Figure 3.3 Data-flow model of the global process for the multi-points inspection approach.

3.2.2   Calculation of kinematic parameters

The kinematic parameters, which are the position and the instantaneous velocity of the inspected point, are calculated independently for each view. In order to calculate the 3D coordinates of the inspected point, it is necessary first to determine the camera matrix, then to establish the correspondence of the sphere image center in the two images appearing in the two cameras. The method of determination of the camera matrices are presented in Section 2.2.3.1. Because projection of the emitting sphere is the circular area, the gravity center of the pixels forming the image of this area is considered as the sphere image center.

The coordinates of the center of the sphere image $[u_{sc}, v_{sc}]$ are calculated using the following formula:

$$\begin{cases} u_{sc} = \dfrac{\displaystyle\sum_{i=1}^{n} u_i}{n} \\ v_{sc} = \dfrac{\displaystyle\sum_{i=1}^{n} v_i}{n} \end{cases} \tag{3.2}$$

where

u_i, v_i are coordinates of the ith pixel having value "one" pixel in the binary image.

n is the total of pixels having value "one" in the binary image.

The sphere image center is used as the corresponding feature. Keep in mind, the image of each sphere in two cameras was already identified in the extraction process. After determination of the correspondence, one can determine the 3D coordinates of the center of the emitting sphere and calculate the corresponding instantaneous velocity using the method presented previously in Section 2.2.3.

3.2.3   Establishment of the flexible interdiction zone

The camera set tracks the movement of the inspected points. If the instantaneous velocity of an inspected point intersects the initial interdiction zone, a corresponding flexible interdiction zone is generated. The necessary formula to calculate the change in dimensions and the form of the flexible interdiction zone is presented in Section 2.2.4.

3.2.4   Verification of the interference between the inspected point and the flexible interdiction zone

For each camera set, every moving (non-hidden) inspected point establishes a corresponding flexible interdiction. The activation of the stop signal depends on the interference between these two elements. This interference is verified using the spatial traversability vector. If the

inspected point is inside the corresponding flexible interdiction zone, the corresponding spatial traversability vector will have a known value. At this moment, the stop signal reasoned by this interference is activated.

Keeping in mind that there are as many inspected points as the number of the emitting spheres on the bracelet; and each inspected point can generate a stop signal in case of interference. The first activated stop signal will stop the machine.

3.3   Experimental

3.3.1   Test bench

The test bench was modified in order to work with the multi-point inspection system. Figure 3.4 shows the modified test bench. The main difference is in the vision system that consisted of two digital stereo heads, filters, and the emitting spheres (color electrical bulbs) which were fixed on the mechanical hands.
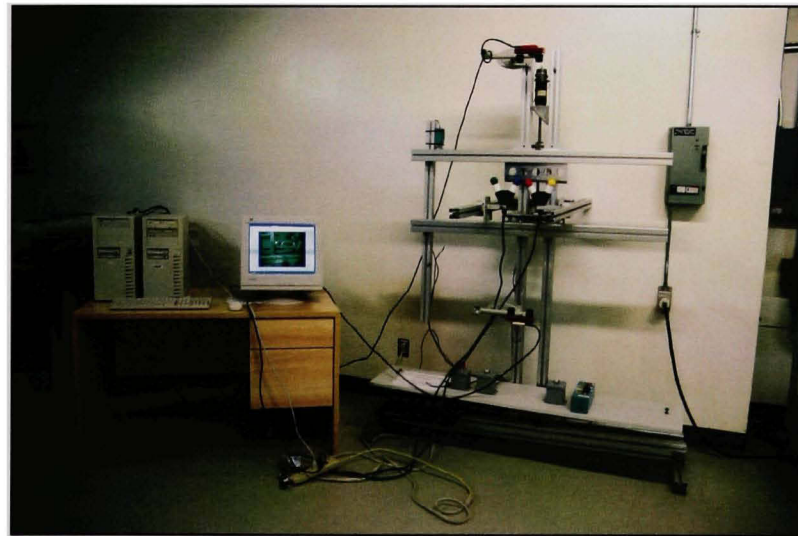

Figure 3.4   The modified test bench.

Figure 3.5 shows a mechanical hand equipped with two electrical bulbs of different colors.

Figure 3.5   The emitting spheres.

3.3.1.1   The processing time

The average time for a global processing cycle per sphere, without considering the image acquisition time, was 0.2s with 640×480 pixels resolution.

3.3.2   The extraction process

The first step of the global process is extraction of the spheres from the captured image. Figure 3.6 presents the spheres and their corresponding binary images after the extraction process. The experiment was performed with a mechanical hand. In this case, a sphere is occulted by the wrist.


(a)   (b)   (c)   (d)
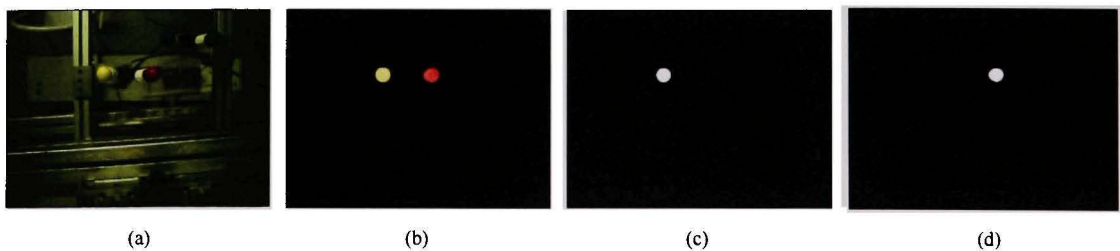
Figure 3.6   The extraction process.

(a) the actual emitting spheres.
(b) the filtered image of the emitting spheres.
(c) (d) the corresponding images of the emitting spheres after the extraction process.

It was observed that with this multi-point inspection system it is possible to track many inspected points at the same time. Figure 3.6 shows that in the case of three emitting spheres, it was possible to identify two of them.

3.4   Results

3.4.1   Investigation of the error of positioning

As with single-point inspection, it is necessary to investigate the error of positioning method. The devices and the performing steps are almost the same as in Section 2.4.1 . Figure 3.7 shows the experimental set-up.
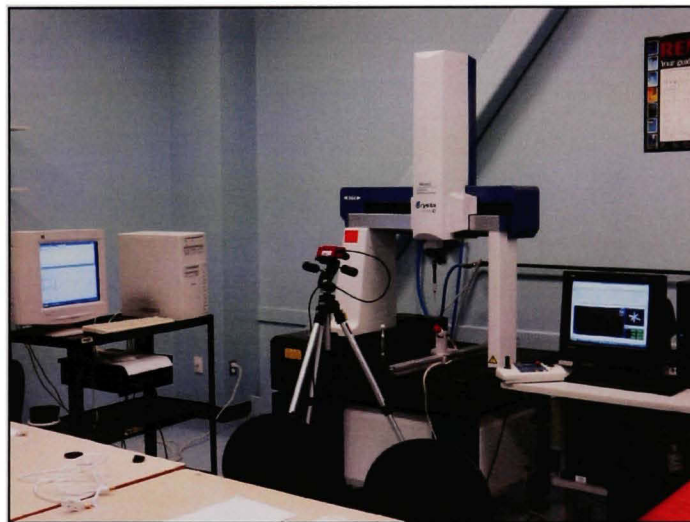

Figure 3.7   The experimental set-up for assessment of the error of positioning.

In this experiment, the emitting bracelet in Section 2.4.1 was replaced by an emitting sphere placed on the table of the CMM. The arrangement of the vision system and the CMM were unchanged. Table 3.1 illustrates the difference between the coordinates of the center of the sphere measured by the CMM and the results obtained by the vision system in various distances and resolutions.

Table 3.1

The difference between the coordinates measured by the coordinate measuring machine and the results obtained by the vision system in various distances and resolutions.

Distance	Measured by the CMM $[x, y, z]^*$ (1)	Resolution 1280×960 $[x, y, z]^*$ (2)	Resolution 640×480 $[x, y, z]^*$ (3)	Difference** $[\Delta x, \Delta y, \Delta z]^*$ (4) = (1) – (2)	Difference** $[\Delta x, \Delta y, \Delta z]^*$ (5) = (1) – (3)
~700 mm	[366±0.5, 53±0.5, 209±0.5]	[368±0.3, 59±0.5, 206±0.3]	[369±0.3, 67±0.5, 202±0.3]	[-2, -6, 3]	[-3, -14, 7]
~800 mm	[366±0.5, 176±0.5, 209±0.5]	[367±0.3, 181±0.5, 207±0.3]	[368±0.3, 185±0.5, 203±0.3]	[-1, -5, 2]	[-2, -9, 6]
~900 mm	[366±0.5, 279±0.5, 209±0.5]	[367±0.3, 283±0.5, 207±0.3]	[369±0.3, 291±0.5, 202±0.3]	[-1, -4, 2]	[-3, -12, 7]
~1000 mm	[366±0.5, 375±0.5, 209±0.5]	[368±0.3, 383±0.5, 206±0.3]	[371±0.3, 392±0.5, 200±0.3]	[-2, -8, 3]	[-5, -17, 9]

* in mm

** difference between the mean values

The results in Table 3.1 show the influence of the distance separating the stereo head and the sphere, and the influence of the image resolution on the precision of the positioning method. The first factor plays a negative role, whereas the second factor is directly proportional to the precision. Comparing Table 3.1 and Table 2.3 confirms the superiority of the second approach where the center of the emitting sphere was used as the inspected point, instead of the center of the emitting bracelet. It was demonstrated [22] that in certain specific situation, the location of the bracelet image center (the center of the approximated ellipse) did not coincide with the projection of the bracelet center.

3.4.2   Investigation of the error of the velocity magnitude

Similar to Section 2.4.2, the error of the velocity magnitude of the inspected point was performed by comparing the velocity magnitude of the center of the sphere by two different methods.

Figure 3.8 shows the experimental set-up allowing comparing of a known velocity of the inspected point with the results calculated by the vision system. In this experiment, an emitting sphere was placed on the table of the motorized linear positioner with controllable

speed. The working resolution for the stereo head was fixed at 640×480. The difference of the velocity magnitude was verified with the various distances between the emitting sphere and the stereo head. Table 3.2 illustrates the difference between the velocity set on the linear positioner and the results obtained from the vision system.
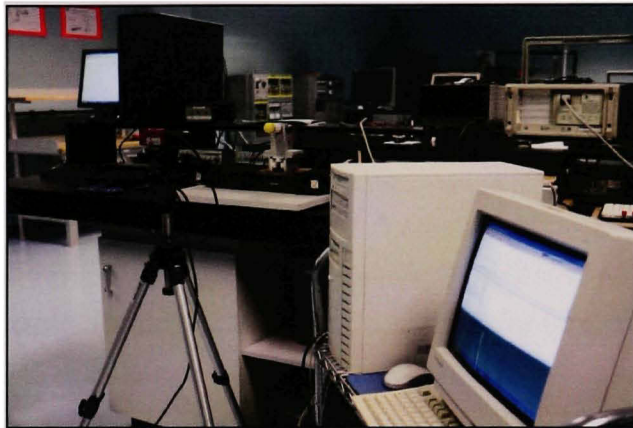
Figure 3.8   The experimental set-up for the assessment of the error of the velocity magnitude of the sphere.

Table 3.2
The difference between the velocity magnitude of the emitting sphere set on the positioner and the results obtained using the vision system in various distances with the resolution of 640×480 pixels.

Distance	The velocity magnitude set on the linear positioner (mm/s)	The minimum and the maximum value of the calculated velocity magnitude (mm/s)	The number of measurement
~400 mm	8	7.9 - 8.1	50
~500 mm	8	8.2 - 8.4	50
~700 mm	8	8.4 - 8.6	50
~900 mm	8	8.7 - 8.9	50

Column (3) of Table 3.2 shows that the precision of the measured velocity magnitude decreases with the distance between the stereo head and the emitting sphere. It is also observed that the difference between the maximum and the minimum values is smaller for this approach, in comparison with the previous one. Again, this amelioration might come from the better precision of the y coordinate in the positioning step.

3.5 Conclusion

Chapter three presents the investigation of a different approach for the flexible protective system for press-brakes with multi-point scheme. In this system, the movement of each worker's hand is inspected by some inspected points attached on the wrist. Precision is higher when the inspected point is the center of the emitting sphere, than when it is the center of the emitting bracelet. The disadvantage of the approach lies in the increase in processing time due to the increase in the number of the inspected points.

CONCLUSION

The purpose of this thesis is to present a new principle, primarily aimed to improve existing protective systems for hydraulic press-brakes. The new system must have the ability to recognize situations in which it is not necessary to stop the machines, which is lacking in the actual protective systems. The validity of the principle for such a system is proven in Chapters 3 and 4 of the thesis. The new theory is based on determination of the direction of movement of one or several inspected point(s) on the worker's hand. This would serve to eliminate machine stoppage in cases which are not actually dangerous, and also to create a protective zone capable of changing the protection volume according to the velocity of the inspected point, in order to stop the machine appropriately, in cases of increased speed of the inspected point towards the area defined as the dangerous zone.

In order to fulfill this purpose, certain criteria were deemed necessary for the design of the protective system for press-brakes. The criteria are as follows :
- recognition of cases in which the movement of the worker's hand actually poses danger, based on the direction of the velocity of the inspected point;
- usage of the velocity vector of the movement of the inspected point having dangerous direction, to determine the necessary dimensions of the protective zone, in order to make this zone more suitable. The magnitude of the velocity vector of the inspected point is the second factor taken into consideration;
- system must make the decision to stop the machine automatically, based on the relation between the position of the inspected point and the outline of the protective zone.

The experimental results prove the capability of vision technology to determine the kinematic parameters of the inspected point.

Theoretically, two definitions concerning the inspected point have been presented. According to the first definition, the center of the emitting bracelet is the inspected point. In the second definition, the center of the emitting sphere is the inspected point. Both methods permit

capturing the image of the emitting bracelet and the emitting sphere on the sensor of the camera in a stable fashion.

Another problem, which has been resolved, is the guarantee that the inspected point be tracked continuously by the protective system. Several camera sets are distributed at viewing locations where there is a possibility that the inspected point may be hidden during machine operation. Specifically, distribution of the camera sets must guarantee continuous inspection of the inspected point by at least one camera set, at all times.

In theory, the form of the flexible protective zone is decided based on the direction of the velocity vector of the inspected point. Equation (2.9) is proposed for determination of this zone. This equation integrates the velocity vector of the inspected point, as well as the constants relating to the process of stopping the machine punch, into the establishment of the flexible protective zone.

The mathematical tool used for making the decision to stop the machine, namely traversibility vector, has been modified for application in 3D situations. This tool is used to verify the entry of the inspected point into the protective zone and simplifies the task of verification.

Concerning the investigation of the error of positioning, the results measured by visual method were verified with the values measured by CMM of Mitutoyo. For the investigation of the error of magnitude of the velocity vector, the results measured by visual technique were also verified with the results measured by the positioner.

In the case of the emitting bracelet, measurement of the position of the inspected point using the vision technique, at a distance of 900mm, under 1280x960 pixels resolution, demonstrated a difference of 10mm on the y coordinate, compared with the value measured by CMM. In the method using the emitting sphere, this difference was 4mm. In addition, the

experiments also show that the resolution of the camera is an important factor in increasing precision. Increasing the resolution significantly improves the precision of location.

The average magnitude of the velocity vector, measured using vision technology, with the emitting bracelet at a distance of 900mm, under 640x480 pixels resolution, had a difference of 9% compared with the set speed of the positioner. In the method using the emitting sphere, this difference was 10%.

Tends of development

The proposed protective system is presented by the approaches and the primary experiments. Even though the prospects applying the system in practice, it could be upgraded in future according to some directions as follows :
- improvement of the processing time of the system;
- manufacture of the glove attaching the emitting bracelets or the emitting spheres.

APPENDIX I

SHAPES OF THE FLEXIBLE INTERDICTION ZONE

Instantaneous vectors and the corresponding flexible interdiction zones, the black lines represent the initial interdiction zone, while the bold lines (both blue and black) represent the flexible interdiction zone.
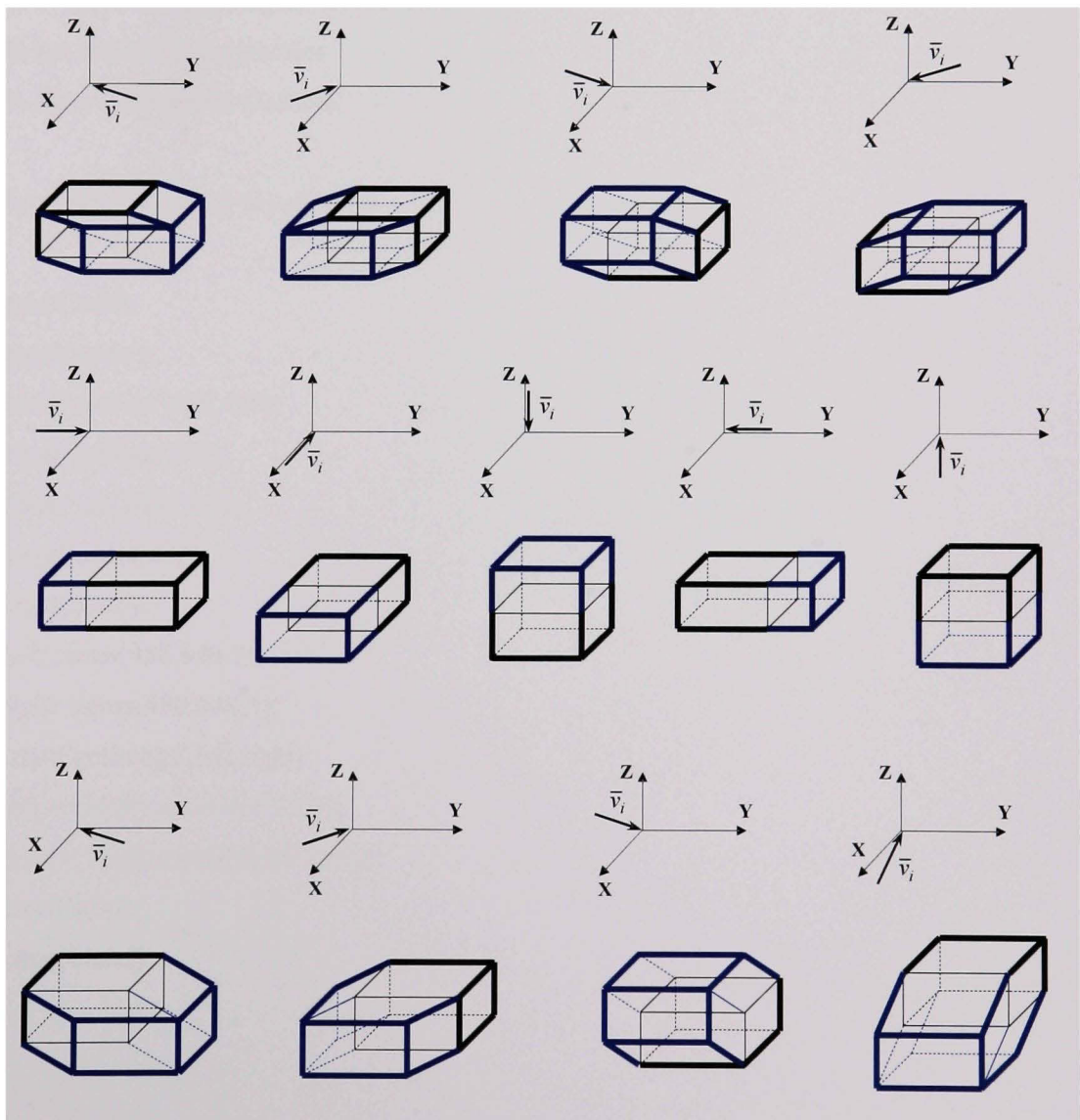
APPENDIX II

SOURCE CODE OF FUNCTIONS

Capture images

% Capture 2 images of the stereo head

% Set the initial parameters

% Save 2 images to matrices

```
function [left,right]=layanhSVS

cmat('init');
cmat('open');
cmat('setSize',640,480);
cmat('setRate',30);
cmat('setColor',1,1);
cmat('setRect',1);
cmat('start');
left=zeros(480,640,3);
right=zeros(480,640,3);
cmat('getImage',left,right);
left = uint8(round(left*255));
right = uint8(round(right*255));
cmat('stop');
cmat('close');
```

Extraction of the emitting object by the method of color threshold

```
% Extract objects to the binary images
% Known thresholds

function [Output_image1,Output_image2]=tachobject(left,right)

r1=left(:,:,1);
g1=left(:,:,2);
b1=left(:,:,3);
Output_image1 = roicolor(r1,200,255).*roicolor(g1,100,180).*roicolor(b1,30,120);
r2=right(:,:,1);
g2=right(:,:,2);
b2=right(:,:,3);
Output_image2 = roicolor(r2,200,255).*roicolor(g2,100,180).*roicolor(b2,30,120);
```

Determination of the coordinates of the center of the fitting ellipse

```
% Approximating bracelet to an ellipse
% Determining the center of the ellipse

function [Cx,Cy]=tinhtoadotamellipse_fitting(Output_image_f)

% Build the design matrix

[m,n]=size(Output_image_f);
ee=0;
for i=1:m
    for j=1:n
        if (Output_image_f(i,j)~=0)
```

```
        ee=ee+1;
        D1(ee,1)=i^2;
        D1(ee,2)=i*j;
        D1(ee,3)=j^2;
        D2(ee,1)=i;
        D2(ee,2)=j;
        D2(ee,3)=1;
    end
  end
end


%   Build the scatter matrix

S1=D1'*D1;
S2=D1'*D2;
S3=D2'*D2;


% T,M

T=- inv(S3)*S2';
M=S1+S2*T;
M=[M(3,:) ./ 2; -M(2,:);M(1,:) ./ 2];


%   Eigenvalues , Calcul a

[evec,eval]=eig(M);
cond=4*evec(1,:) .* evec(3,:) - evec(2,:) .^2;
a1=evec(:, find(cond>0));
a=[a1;T*a1];
```

% Center coordinate C(Cx,Cy)

Cx=((a(2)*a(5)-2*a(3)*a(4))/(4*a(1)*a(3)-(a(2)^2)));
Cy=((a(2)*a(4)-2*a(1)*a(5))/(4*a(1)*a(3)-(a(2)^2)));

Determination of the camera matrices

% Determining 2 camera matrices of the stereo head
% Input data

% 3D coordinates of the calibration object
x=[149.6 60.9 60.9 149.6 149.4 60.7 60.9 149.4 150.5 61.8 61.8 150.5 150.7 62 62 150.7 151.7 62 63.3 152 152.6 64.1 64.2 153];
y=[36.7 36.7 63 62.2 96.3 96.7 121.6 121.7 155.2 155.6 181.5 180.7 245.9 246.9 272.7 271.9 310.3 311.3 337 336 370.7 371.4 397 396.5];
z=[86.3 85.9 93.9 93.9 104.7 104.8 113 113 124 123.5 132 132.1 133.4 133.3 125.2 125.4 113 112.8 104.5 104.8 93.6 93.4 85.6 85.9];

% 2D location of the corners of the left camera
u1=[540 540 518 519 490 488 464 465 433 433 405 406 336 336 305 306 267 266 238 239 206 205 180 180];   %Left
v1=[197 286 286 196 195 289 289 195 193 290 290 193 192 290 290 192 192 287 286 192 192 284 283 192];

% 2D location of the corners of the right camera
u2=[474 474 448 450 418 416 390 390 356 356 326 327 256 255 228 228 192 190 166 165 136 135 111 111];   %Right
v2=[183 273 275 182 181 276 276 181 179 277 278 179 178 277 276 178 178 273 272 178 178 269 268 178];

```
n=24;
j=1;

% Transform matrix of 1st camera

for i=1:n
    A1(j,:)=[x(i) y(i) z(i) 1 0 0 0 0 -(x(i)*u1(i)) -(y(i)*u1(i)) -(z(i)*u1(i))];
    A1(j+1,:)=[0 0 0 0 x(i) y(i) z(i) 1 -(x(i)*v1(i)) -(y(i)*v1(i)) -(z(i)*v1(i))];
    B1(j)=u1(i);
    B1(j+1)=v1(i);
    j=2*i+1;
end
C1=(inv(A1'*A1))*A1'*(B1');
R1=B1'-A1*C1;


% Transform matrix of 2nd camera

j=1;
for i=1:n
    A2(j,:)=[x(i) y(i) z(i) 1 0 0 0 0 -(x(i)*u2(i)) -(y(i)*u2(i)) -(z(i)*u2(i))];
    A2(j+1,:)=[0 0 0 0 x(i) y(i) z(i) 1 -(x(i)*v2(i)) -(y(i)*v2(i)) -(z(i)*v2(i))];
    B2(j)=u2(i);
    B2(j+1)=v2(i);
    j=2*i+1;
end
C2=(inv(A2'*A2))*A2'*(B2');
R2=B2'-A2*C2;
```

<u>Determination of the 3D coordinates of the inspected point</u>

% 3D coordinates of the inspected point was determined by using 2D ellipse center coordinates and the camera matrices

function [TD]=tinhtoado3D(Cxl,Cyl,Cxr,Cyr)

```
uu(1) = Cyl;
vv(1) = Cxl;
uu(2) = Cyr;
vv(2) = Cxr;
```

% 3D coordinates
% Points P1(z=3), P2(z=10)

```
ATC1=[C1(1)-C1(9)*uu(1) C1(2)-C1(10)*uu(1); C1(5)-C1(9)*vv(1) C1(6)-C1(10)*vv(1)];
BTC1=[uu(1)-C1(4)-(C1(3)-C1(11)*uu(1))*3; vv(1)-C1(8)-(C1(7)-C1(11)*vv(1))*3];
XTC1=(inv(ATC1))*BTC1;
P1=[XTC1(1);XTC1(2);3];
```

```
ATC1=[C1(1)-C1(9)*uu(1) C1(2)-C1(10)*uu(1); C1(5)-C1(9)*vv(1) C1(6)-C1(10)*vv(1)];
BTC1=[uu(1)-C1(4)-(C1(3)-C1(11)*uu(1))*10; vv(1)-C1(8)-(C1(7)-C1(11)*vv(1))*10];
XTC1=(inv(ATC1))*BTC1;
P2=[XTC1(1);XTC1(2);10];
```

```
P1P2=P2-P1;
```

% Points Q1(z=3), Q2(z=10)

```
ATC2=[C2(1)-C2(9)*uu(2) C2(2)-C2(10)*uu(2); C2(5)-C2(9)*vv(2) C2(6)-C2(10)*vv(2)];
BTC2=[uu(2)-C2(4)-(C2(3)-C2(11)*uu(2))*3; vv(2)-C2(8)-(C2(7)-C2(11)*vv(2))*3];
```

```
XTC2=(inv(ATC2))*BTC2;
Q1=[XTC2(1); XTC2(2);3];


ATC2=[C2(1)-C2(9)*uu(2) C2(2)-C2(10)*uu(2); C2(5)-C2(9)*vv(2) C2(6)-C2(10)*vv(2)];
BTC2=[uu(2)-C2(4)-(C2(3)-C2(11)*uu(2))*10; vv(2)-C2(8)-(C2(7)-C2(11)*vv(2))*10];
XTC2=(inv(ATC2))*BTC2;
Q2=[XTC2(1); XTC2(2);10];
Q1Q2=Q2-Q1;


% Calculation of a1, a2


P1Q1=Q1-P1;
AF=[dot(P1P2,P1P2) -(dot(P1P2,Q1Q2));dot(P1P2,Q1Q2) -(dot(Q1Q2,Q1Q2))];
BF=[dot(P1Q1,P1P2);dot(P1Q1,Q1Q2)];
XF=(inv(AF))*BF;
a1=XF(1);
a2=XF(2);


% 3D coordinates


V=P1 + a1*P1P2 -(Q1 + a2*Q1Q2);
% V: shortest vector connecting the two lines


MV=sqrt(dot(V,V))
% Module of V for verifying error in corresponding image points


TD=0.5*((P1+a1*P1P2) + (Q1+a2*Q1Q2));
% Display coordinates of the inspected point (3D coordinates)
```

Verification of the condition intersection of the instantaneous vector of the inspected point with the initial interdiction zone

```
function [cat]=check(x1,y1,z1,x2,y2,z2,iz_x,iz_y,iz_z)

%  Data of 6 planes

a=iz_x;    % plan intersect with x axes
b=iz_y;    % plan intersect with y axes
c=iz_z;    % plan intersect with z axes

x(1)=x1;
y(1)=y1;
z(1)=z1;

x(2)=x2;
y(2)=y2;
z(2)=z2;

%  Check of intersection

dk=0;

% dk=1 having intersection , dk=0 not intersecting between vector and one of five planes
% MP1: z=0 , 0 <= x <=a , 0 <= y <=b

xmp1=x(1) + (x(2)-x(1))*(-z(1))/(z(2)-z(1));
ymp1=y(1) + (y(2)-y(1))*(-z(1))/(z(2)-z(1));
if (0<=xmp1)&(xmp1<=a)&(0<=ymp1)&(ymp1<=b) dk(1)=1; else dk(1)=0; end
```

```
% MP2: y=b , 0 <= x <=a , 0 <= z <=c


xmp2=x(1) + (x(2)-x(1))*(b-y(1))/(y(2)-y(1));
zmp2=z(1) + (z(2)-z(1))*(b-y(1))/(y(2)-y(1));
if (0<=xmp2)&(xmp2<=a)&(0<=zmp2)&(zmp2<=c) dk(2)=1; else dk(2)=0; end


% MP3: z=c , 0 <= x <=a , 0 <= y <=b


xmp3=x(1) + (x(2)-x(1))*(c-z(1))/(z(2)-z(1));
ymp3=y(1) + (y(2)-y(1))*(c-z(1))/(z(2)-z(1));
if (0<=xmp3)&(xmp3<=a)&(0<=ymp3)&(ymp3<=b) dk(3)=1; else dk(3)=0; end


% MP4: y=0 , 0 <= x <=a , 0 <= z <=c


xmp4=x(1) + (x(2)-x(1))*(-y(1))/(y(2)-y(1));
zmp4=z(1) + (z(2)-z(1))*(-y(1))/(y(2)-y(1));
if (0<=xmp4)&(xmp4<=a)&(0<=zmp4)&(zmp4<=c) dk(4)=1; else dk(4)=0; end


% MP5: x=a , 0 <= y <=b , 0 <= z <=c


ymp5=y(1) + (y(2)-y(1))*(a-x(1))/(x(2)-x(1));
zmp5=z(1) + (z(2)-z(1))*(a-x(1))/(x(2)-x(1));
if (0<=ymp5)&(ymp5<=b)&(0<=zmp5)&(zmp5<=c) dk(5)=1; else dk(5)=0; end


if (dk(1)==0)&(dk(2)==0)&(dk(3)==0)&(dk(4)==0)&(dk(5)==0) cat=0; else cat=1; end


end
```

Establishment of the flexible interdiction zone

% Calculation of new coordinates of a point establishing the flexible interdiction zone

% citx x coordinate of the vector of dimension change

% i is the case corresponding to the direction of the instantaneous vector of the inspected point

% a,b,c is 3 dimensions of the initial interdiction zone

```
function [dnx,dny,dnz]=toadomoi(citx,city,citz,i,a,b,c)

% New coordinates

switch i
  case 1
    dnx=-citx + a;
    dny=-city;
    dnz=-citz;
  case 2
    dnx=-citx + a;
    dny=-city + b;
    dnz=-citz;
  case 3
    dnx=-citx + a;
    dny=-city + b;
    dnz=-citz + c;
  case 4
    dnx=-citx + a;
    dny=-city;
    dnz=-citz + c;
  case 5
```

```
        dnx=-citx;
        dny=-city;
        dnz=-citz;
    case 6
        dnx=-citx;
        dny=-city + b;
        dnz=-citz;
    case 7
        dnx=-citx;
        dny=-city + b;
        dnz=-citz + c;
    case 8
        dnx=-citx;
        dny=-city;
        dnz=-citz + c;
end


function [vecint,xdirec,ydirec,zdirec]=vectorflexible(x1,y1,z1,x2,y2,z2,ti)


% Data
% Coordinates of 2 points creating the displacement vector of the inspected point


x(1)=x1;
y(1)=y1;
z(1)=z1;
x(2)=x2;
y(2)=y2;
z(2)=z2;


t=ti;
```

% The interval time performing the displacement of the inspected point

```
t_response=0.18;    % Response time of the stop system
t_img=0.2;          % Maximum processing time of vision
k=1;
```

% Tinh vector flexible

```
vit=[(x2-x1)/t;(y2-y1)/t;(z2-z1)/t];
% Velocity vector
```

```
m_vit=sqrt(dot(vit,vit));
% Magnitude of velocity vector
```

```
m_cit=k*(t_response+ t_img)*m_vit ;
% Magnitude of the dimension change vector
```

```
vecint=m_cit;
% Dimension change vector
```

```
xdirec=(x2-x1)/(t*m_vit);
ydirec=(y2-y1)/(t*m_vit);
zdirec=(z2-z1)/(t*m_vit);
% Direction of the dimension change vector (normaled)
```

Verification of the interference between the inspected point and the flexible interdiction zone

```
function [stop]=check_inside_flexible(x1,y1,z1,x2,y2,z2,ti,iz_x,iz_y,iz_z)
```

```
% Input
a=iz_x;
b=iz_y;
c=iz_z;


x(1)=x1;
y(1)=y1;
z(1)=z1;


x(2)=x2;
y(2)=y2;
z(2)=z2;


t=ti;


% Code_cit


code_cit=10;
dk=0;
cit=[(x2-x1)/t;(y2-y1)/t;(z2-z1)/t];
citt=[0;0;0];


for i=1:3
   if (cit(i)<0) citt(i)=-1; end
   if (cit(i)>0) citt(i)=1; end
end


[cat]=check(x1,y1,z1,x2,y2,z2,a,b,c)
% cat=1 having intersection, cat=0 not intersecting between vector and one of five planes
```

```
switch cat
   case 1
      if citt==[-1;0;0] code_cit=1;
      elseif citt==[-1;1;1] code_cit=2;
      elseif citt==[-1;1;-1] code_cit=3;
      elseif citt==[0;1;0] code_cit=4;
      elseif citt==[0;0;-1] code_cit=5;
      elseif citt==[-1;-1;1] code_cit=6;
      elseif citt==[-1;-1;-1] code_cit=7;
      elseif citt==[0;-1;0] code_cit=8;
      elseif citt==[0;0;1] code_cit=9;
      elseif citt==[-1;1;0] code_cit=10;
      elseif citt==[-1;-1;0] code_cit=11;
      elseif citt==[-1;0;-1] code_cit=12;
      elseif citt==[-1;0;1] code_cit=13;
      else code_cit=14; end
   otherwise
      code_cit=14;
end


%  Check condition of interference
% Code values of cit , having 27 cases of cit , only consider with
% 8 cases, those cases when it is considered that the flexible dangerous zone is the initial
interdiction zone

switch code_cit
   case 1
      [vecint,xdirec,ydirec,zdirec]=vectorflexible(x1,y1,z1,x2,y2,z2,ti);
      cit=[vecint*xdirec;vecint*ydirec;vecint*zdirec];
```

```
[dnx1,dny1,dnz1]=toadomoi(cit(1),cit(2),cit(3),1,a,b,c);
[dnx2,dny2,dnz2]=toadomoi(cit(1),cit(2),cit(3),2,a,b,c);
[dnx3,dny3,dnz3]=toadomoi(cit(1),cit(2),cit(3),3,a,b,c);
[dnx4,dny4,dnz4]=toadomoi(cit(1),cit(2),cit(3),4,a,b,c);


[a1]=diem_matphang(x(2),y(2),z(2),a,0,0,a,b,0,0,b,0);
[a2]=diem_matphang(x(2),y(2),z(2),a,b,c,a,b,0,0,b,0);
[a3]=diem_matphang(x(2),y(2),z(2),a,0,c,a,b,c,0,b,c);
[a4]=diem_matphang(x(2),y(2),z(2),a,0,0,a,0,c,0,0,c);

[anf5]=diem_matphang(x(2),y(2),z(2),dnx1,dny1,dnz1,dnx2,dny2,dnz2,dnx3,dny3,dnz3);

[a6]=diem_matphang(x(2),y(2),z(2),0,b,0,0,b,c,0,0,c);
if (0<a1)&(0>a2)&(0>a3)&(0>a4)&(0>anf5)&(0<a6) dk=1; else dk=0; end

% dk=1
% inside

  case 2
    [vecint,xdirec,ydirec,zdirec]=vectorflexible(x1,y1,z1,x2,y2,z2,ti);
    cit=[vecint*xdirec;vecint*ydirec;vecint*zdirec]

    [dnx1,dny1,dnz1]=toadomoi(cit(1),cit(2),cit(3),1,a,b,c);
    [dnx2,dny2,dnz2]=toadomoi(cit(1),cit(2),cit(3),2,a,b,c);
    [dnx3,dny3,dnz3]=toadomoi(cit(1),cit(2),cit(3),3,a,b,c);
    [dnx4,dny4,dnz4]=toadomoi(cit(1),cit(2),cit(3),4,a,b,c);
    [dnx5,dny5,dnz5]=toadomoi(cit(1),cit(2),cit(3),5,a,b,c);
    [dnx6,dny6,dnz6]=toadomoi(cit(1),cit(2),cit(3),6,a,b,c);
    [dnx8,dny8,dnz8]=toadomoi(cit(1),cit(2),cit(3),8,a,b,c);
```

```
[a2]=diem_matphang(x(2),y(2),z(2),a,b,0,a,b,c,0,b,c);
[a3]=diem_matphang(x(2),y(2),z(2),a,b,c,a,0,c,0,0,c);
[a6]=diem_matphang(x(2),y(2),z(2),0,b,0,0,b,c,0,0,c);


[anl4]=diem_matphang(x(2),y(2),z(2),dnx5,dny5,dnz5,dnx8,dny8,dnz8,dnx4,dny4,dnz4);
[anl6]=diem_matphang(x(2),y(2),z(2),dnx5,dny5,dnz5,dnx8,dny8,dnz8,0,0,c);
[anl3]=diem_matphang(x(2),y(2),z(2),dnx4,dny4,dnz4,dnx8,dny8,dnz8,0,0,c);


[anf2]=diem_matphang(x(2),y(2),z(2),dnx2,dny2,dnz2,dnx3,dny3,dnz3,a,b,c);
[anf3]=diem_matphang(x(2),y(2),z(2),dnx3,dny3,dnz3,dnx4,dny4,dnz4,a,0,c);
[anf5]=diem_matphang(x(2),y(2),z(2),dnx1,dny1,dnz1,dnx2,dny2,dnz2,dnx3,dny3,dnz3);


[and1]=diem_matphang(x(2),y(2),z(2),dnx1,dny1,dnz1,dnx2,dny2,dnz2,dnx6,dny6,dnz6);
[and2]=diem_matphang(x(2),y(2),z(2),dnx2,dny2,dnz2,dnx6,dny6,dnz6,0,b,0);
[and6]=diem_matphang(x(2),y(2),z(2),dnx5,dny5,dnz5,dnx6,dny6,dnz6,0,b,0);


    if
(0<a2)&(0<a3)&(0<a6)&(0<anl4)&(0>anl6)&(0<anl3)&(0<anf2)&(0<anf3)&(0>anf5)&(0<
and1)&(0>and2)&(0<and6) dk=1; else dk=0; end

  case 3
    [vecint,xdirec,ydirec,zdirec]=vectorflexible(x1,y1,z1,x2,y2,z2,ti);
    cit=[vecint*xdirec;vecint*ydirec:vecint*zdirec];


    [dnx1,dny1,dnz1]=toadomoi(cit(1),cit(2),cit(3),1,a,b,c);
    [dnx2,dny2,dnz2]=toadomoi(cit(1),cit(2),cit(3),2,a,b,c);
    [dnx3,dny3,dnz3]=toadomoi(cit(1),cit(2),cit(3),3,a,b,c);
    [dnx4,dny4,dnz4]=toadomoi(cit(1),cit(2),cit(3),4,a,b,c);
```

```
[dnx5,dny5,dnz5]=toadomoi(cit(1),cit(2),cit(3),5,a,b,c);
[dnx7,dny7,dnz7]=toadomoi(cit(1),cit(2),cit(3),7,a,b,c);
[dnx8,dny8,dnz8]=toadomoi(cit(1),cit(2),cit(3),8,a,b,c);


[a1]=diem_matphang(x(2),y(2),z(2),a,0,0,a,b,0,0,b,0);
[a2]=diem_matphang(x(2),y(2),z(2),a,b,0,a,b,c,0,b,c);
[a6]=diem_matphang(x(2),y(2),z(2),0,b,0,0,b,c,0,0,c);


[anu2]=diem_matphang(x(2),y(2),z(2),dnx3,dny3,dnz3,dnx7,dny7,dnz7,0,b,c);
[anu3]=diem_matphang(x(2),y(2),z(2),dnx3,dny3,dnz3,dnx7,dny7,dnz7,dnx8,dny8,dnz8);
[anu6]=diem_matphang(x(2),y(2),z(2),dnx7,dny7,dnz7,dnx8,dny8,dnz8,0,0,c);


[anl1]=diem_matphang(x(2),y(2),z(2),dnx1,dny1,dnz1,dnx5,dny5,dnz5,0,0,0);
[anl4]=diem_matphang(x(2),y(2),z(2),dnx5,dny5,dnz5,dnx8,dny8,dnz8,dnx4,dny4,dnz4);
[anl6]=diem_matphang(x(2),y(2),z(2),dnx5,dny5,dnz5,dnx8,dny8,dnz8,0,0,c);


[anf1]=diem_matphang(x(2),y(2),z(2),dnx1,dny1,dnz1,dnx2,dny2,dnz2,a,b,0);
[anf2]=diem_matphang(x(2),y(2),z(2),dnx2,dny2,dnz2,dnx3,dny3,dnz3,a,b,c);
[anf5]=diem_matphang(x(2),y(2),z(2),dnx1,dny1,dnz1,dnx2,dny2,dnz2,dnx3,dny3,dnz3)


    if
(0<a1)&(0<a2)&(0<a6)&(0<anu2)&(0>anu3)&(0<anu6)&(0>anl1)&(0<anl4)&(0>anl6)&(0
<anf1)&(0<anf2)&(0>anf5) dk=1; else dk=0; end

  case 4
    [vecint,xdirec,ydirec,zdirec]=vectorflexible(x1,y1.z1,x2,y2,z2,ti);
    cit=[vecint*xdirec;vecint*ydirec;vecint*zdirec];


    [dnx1,dny1,dnz1]=toadomoi(cit(1),cit(2),cit(3),1,a,b,c);
    [dnx4,dny4,dnz4]=toadomoi(cit(1),cit(2),cit(3),4,a,b,c);
```

```
[dnx8,dny8,dnz8]=toadomoi(cit(1),cit(2),cit(3),8,a,b,c);

[a1]=diem_matphang(x(2),y(2),z(2),a,0,0,a,b,0,0,b,0);
[a2]=diem_matphang(x(2),y(2),z(2),a,b,c,a,b,0,0,b,0);
[a3]=diem_matphang(x(2),y(2),z(2),a,0,c,a,b,c,0,b,c);

[anl4]=diem_matphang(x(2),y(2),z(2),dnx1,dny1,dnz1,dnx4,dny4,dnz4,dnx8,dny8,dnz8);

[a5]=diem_matphang(x(2),y(2),z(2),a,0,c,a,b,0,a,b,c);
[a6]=diem_matphang(x(2),y(2),z(2),0,b,0,0,b,c,0,0,c);

if (0<a1)&(0>a2)&(0>a3)&(0>anl4)&(0>a5)&(0<a6) dk=1; else dk=0; end

case 5
    [vecint,xdirec,ydirec,zdirec]=vectorflexible(x1,y1,z1,x2,y2,z2,ti);
    cit=[vecint*xdirec;vecint*ydirec;vecint*zdirec];

    [dnx3,dny3,dnz3]=toadomoi(cit(1),cit(2),cit(3),3,a,b,c);
    [dnx4,dny4,dnz4]=toadomoi(cit(1),cit(2),cit(3),4,a,b,c);
    [dnx7,dny7,dnz7]=toadomoi(cit(1),cit(2),cit(3),7,a,b,c);

    [a1]=diem_matphang(x(2),y(2),z(2),a,0,0,a,b,0,0,b,0);
    [a2]=diem_matphang(x(2),y(2),z(2),a,b,c,a,b,0,0,b,0);

[anu3]=diem_matphang(x(2),y(2),z(2),dnx4,dny4,dnz4,dnx3,dny3,dnz3,dnx7,dny7,dnz7);
    [a4]=diem_matphang(x(2),y(2),z(2),a,0,0,0,0,0,0,0,c);
    [a5]=diem_matphang(x(2),y(2),z(2),a,0,c,a,b,0,a,b,c);
    [a6]=diem_matphang(x(2),y(2),z(2),0,b,0,0,b,c,0,0,c);

    if (0<a1)&(0>a2)&(0>anu3)&(0<a4)&(0>a5)&(0<a6) dk=1; else dk=0; end
```

```
case 6
    [vecint,xdirec,ydirec,zdirec]=vectorflexible(x1,y1,z1,x2,y2,z2,ti);
    cit=[vecint*xdirec;vecint*ydirec;vecint*zdirec];

    [dnx1,dny1,dnz1]=toadomoi(cit(1),cit(2),cit(3),1,a,b,c)
    [dnx2,dny2,dnz2]=toadomoi(cit(1),cit(2),cit(3),2,a,b,c);
    [dnx3,dny3,dnz3]=toadomoi(cit(1),cit(2),cit(3),3,a,b,c);
    [dnx4,dny4,dnz4]=toadomoi(cit(1),cit(2),cit(3),4,a,b,c);
    [dnx5,dny5,dnz5]=toadomoi(cit(1),cit(2),cit(3),5,a,b,c);
    [dnx6,dny6,dnz6]=toadomoi(cit(1),cit(2),cit(3),6,a,b,c);
    [dnx7,dny7,dnz7]=toadomoi(cit(1),cit(2),cit(3),7,a,b,c);

    [a3]=diem_matphang(x(2),y(2),z(2),a,0,c,a,b,c,0,b,c);
    [a4]=diem_matphang(x(2),y(2),z(2),a,0,0,0,0,0,0,0,c);
    [a6]=diem_matphang(x(2),y(2),z(2),0,b,0,0,b,c,0,0,c);

[anr2]=diem_matphang(x(2),y(2),z(2),dnx3,dny3,dnz3,dnx7,dny7,dnz7,dnx6,dny6,dnz6);
[anr3]=diem_matphang(x(2),y(2),z(2),dnx3,dny3,dnz3,dnx7,dny7,dnz7,0,b,c);
[anr6]=diem_matphang(x(2),y(2),z(2),dnx7,dny7,dnz7,dnx6,dny6,dnz6,0,b,0);

[anf3]=diem_matphang(x(2),y(2),z(2),dnx3,dny3,dnz3,dnx4,dny4,dnz4,a,0,c);
[anf4]=diem_matphang(x(2),y(2),z(2),dnx1,dny1,dnz1,dnx4,dny4,dnz4,a,0,c);
[anf5]=diem_matphang(x(2),y(2),z(2),dnx1,dny1,dnz1,dnx2,dny2,dnz2,dnx3,dny3,dnz3);

[and1]=diem_matphang(x(2),y(2),z(2),dnx1,dny1,dnz1,dnx2,dny2,dnz2,dnx6,dny6,dnz6);
[and4]=diem_matphang(x(2),y(2),z(2),dnx1,dny1,dnz1,dnx5,dny5,dnz5,0,0,0);
[and6]=diem_matphang(x(2),y(2),z(2),dnx5,dny5,dnz5,dnx6,dny6,dnz6,0,b,0);
```

```
    if
(0>a3)&(0<a4)&(0<a6)&(0<anr2)&(0>anr3)&(0>anr6)&(0<anf3)&(0>anf4)&(0>anf5)&(0<
and1)&(0<and4)&(0<and6) dk=1; else dk=0; end

  case 7
    [vecint,xdirec,ydirec,zdirec]=vectorflexible(x1,y1,z1,x2,y2,z2,ti);
    cit=[vecint*xdirec;vecint*ydirec;vecint*zdirec];

    [dnx1,dny1,dnz1]=toadomoi(cit(1),cit(2),cit(3),1,a,b,c);
    [dnx2,dny2,dnz2]=toadomoi(cit(1),cit(2),cit(3),2,a,b,c);
    [dnx3,dny3,dnz3]=toadomoi(cit(1),cit(2),cit(3),3,a,b,c);
    [dnx4,dny4,dnz4]=toadomoi(cit(1),cit(2),cit(3),4,a,b,c);
    [dnx6,dny6,dnz6]=toadomoi(cit(1),cit(2),cit(3),6,a,b,c);
    [dnx7,dny7,dnz7]=toadomoi(cit(1),cit(2),cit(3),7,a,b,c);
    [dnx8,dny8,dnz8]=toadomoi(cit(1),cit(2),cit(3),8,a,b,c);

    [a1]=diem_matphang(x(2),y(2),z(2),a,0,0,a,b,0,0,b,0);
    [a4]=diem_matphang(x(2),y(2),z(2),a,0,0,0,0,0,0,0,c);
    [a6]=diem_matphang(x(2),y(2),z(2),0,b,0,0,b,c,0,0,c);

[anr1]=diem_matphang(x(2),y(2),z(2),dnx2,dny2,dnz2,dnx6,dny6,dnz6,0,b,0);
[anr2]=diem_matphang(x(2),y(2),z(2),dnx2,dny2,dnz2,dnx6,dny6,dnz6,dnx7,dny7,dnz7);
[anr6]=diem_matphang(x(2),y(2),z(2),dnx7,dny7,dnz7,dnx6,dny6,dnz6,0,b,0);

[anf1]=diem_matphang(x(2),y(2),z(2),a,b,0,a,0,0,dnx1,dny1,dnz1);
[anf4]=diem_matphang(x(2),y(2),z(2),dnx1,dny1,dnz1,dnx4,dny4,dnz4,a,0,c);
[anf5]=diem_matphang(x(2),y(2),z(2),dnx1,dny1,dnz1,dnx2,dny2,dnz2,dnx3,dny3,dnz3);

[anu3]=diem_matphang(x(2),y(2),z(2),dnx4,dny4,dnz4,dnx3,dny3,dnz3,dnx7,dny7,dnz7);
[anu4]=diem_matphang(x(2),y(2),z(2),dnx4,dny4,dnz4,dnx8,dny8,dnz8,0,0,c);
```

```
[anu5]=diem_matphang(x(2),y(2),z(2),dnx8,dny8,dnz8,dnx7,dny7,dnz7,0,b,c);

    if
(0<a1)&(0<a4)&(0<a6)&(0>anr2)&(0>anr6)&(0<anf1)&(0>anf4)&(0>anf5)&(0>anu3)&(0
>anu4)&(0>anu5) dk=1; else dk=0; end

  case 8
    [vecint,xdirec,ydirec,zdirec]=vectorflexible(x1,y1,z1,x2,y2,z2,ti);
    cit=[vecint*xdirec;vecint*ydirec;vecint*zdirec];

    [dnx2,dny2,dnz2]=toadomoi(cit(1),cit(2),cit(3),2,a,b,c);
    [dnx3,dny3,dnz3]=toadomoi(cit(1),cit(2),cit(3),3,a,b,c);
    [dnx6,dny6,dnz6]=toadomoi(cit(1),cit(2),cit(3),6,a,b,c);

    [a1]=diem_matphang(x(2),y(2),z(2),a,0,0,a,b,0,0,b,0);

[anr2]=diem_matphang(x(2),y(2),z(2),dnx3,dny3,dnz3,dnx2,dny2,dnz2,dnx6,dny6,dnz6);

    [a3]=diem_matphang(x(2),y(2),z(2),a,0,c,a,b,c,0,b,c);
    [a4]=diem_matphang(x(2),y(2),z(2),a,0,0,0,0,0,0,0,c);
    [a5]=diem_matphang(x(2),y(2),z(2),a,0,c,a,b,0,a,b,c);
    [a6]=diem_matphang(x(2),y(2),z(2),0,b,0,0,b,c,0,0,c);

    if (0<a1)&(0>anr2)&(0>a3)&(0<a4)&(0>a5)&(0<a6) dk=1; else dk=0; end

  case 9
    [vecint,xdirec,ydirec,zdirec]=vectorflexible(x1,y1,z1,x2,y2,z2,ti);
    cit=[vecint*xdirec;vecint*ydirec;vecint*zdirec]

    [dnx1,dny1,dnz1]=toadomoi(cit(1),cit(2),cit(3),1,a,b,c);
```

```
[dnx2,dny2,dnz2]=toadomoi(cit(1),cit(2),cit(3),2,a,b,c);
[dnx6,dny6,dnz6]=toadomoi(cit(1),cit(2),cit(3),6,a,b,c);


[and1]=diem_matphang(x(2),y(2),z(2),dnx1,dny1,dnz1,dnx2,dny2,dnz2,dnx6,dny6,dnz6);


[a2]=diem_matphang(x(2),y(2),z(2),a,b,c,a,b,0,0,b,0);
[a3]=diem_matphang(x(2),y(2),z(2),a,0,c,a,b,c,0,b,c);
[a4]=diem_matphang(x(2),y(2),z(2),a,0,0,0,0,0,0,0,c);
[a5]=diem_matphang(x(2),y(2),z(2),a,0,c,a,b,0,a,b,c);
[a6]=diem_matphang(x(2),y(2),z(2),0,b,0,0,b,c,0,0,c);


if (0<and1)&(0>a2)&(0>a3)&(0<a4)&(0>a5)&(0<a6) dk=1; else dk=0; end

case 10
[vecint,xdirec,ydirec,zdirec]=vectorflexible(x1,y1,z1,x2,y2,z2,ti);
cit=[vecint*xdirec;vecint*ydirec;vecint*zdirec]


[dnx1,dny1,dnz1]=toadomoi(cit(1),cit(2),cit(3),1,a,b,c);
[dnx2,dny2,dnz2]=toadomoi(cit(1),cit(2),cit(3),2,a,b,c);
[dnx3,dny3,dnz3]=toadomoi(cit(1),cit(2),cit(3),3,a,b,c);
[dnx4,dny4,dnz4]=toadomoi(cit(1),cit(2),cit(3),4,a,b,c);
[dnx5,dny5,dnz5]=toadomoi(cit(1),cit(2),cit(3),5,a,b,c);
[dnx8,dny8,dnz8]=toadomoi(cit(1),cit(2),cit(3),8,a,b,c);


[a1]=diem_matphang(x(2),y(2),z(2),a,0,0,a,b,0,0,b,0);
% Khong can thiet lam , chi de tao ra convex polygon


[a2]=diem_matphang(x(2),y(2),z(2),a,b,c,a,b,0,0,b,0);
[a3]=diem_matphang(x(2),y(2),z(2),a,0,c,a,b,c,0,b,c);
[a6]=diem_matphang(x(2),y(2),z(2),0,b,0,0,b,c,0,0,c);
```

```
[anl4]=diem_matphang(x(2),y(2),z(2),dnx5,dny5,dnz5,dnx8,dny8,dnz8,dnx4,dny4,dnz4);
[anf2]=diem_matphang(x(2),y(2),z(2),dnx2,dny2,dnz2,dnx3,dny3,dnz3,a,b,c);
[anf5]=diem_matphang(x(2),y(2),z(2),dnx1,dny1,dnz1,dnx2,dny2,dnz2,dnx3,dny3,dnz3);

    if (0<a1)&(0>a2)&(0>a3)&(0<a6)&(0<anl4)&(0<anf2)&(0>anf5) dk=1; else dk=0; end

case 11
    [vecint,xdirec,ydirec,zdirec]=vectorflexible(x1,y1,z1,x2,y2,z2,ti);
    cit=[vecint*xdirec;vecint*ydirec;vecint*zdirec];

    [dnx1,dny1,dnz1]=toadomoi(cit(1),cit(2),cit(3),1,a,b,c);
    [dnx2,dny2,dnz2]=toadomoi(cit(1),cit(2),cit(3),2,a,b,c);
    [dnx3,dny3,dnz3]=toadomoi(cit(1),cit(2),cit(3),3,a,b,c);
    [dnx4,dny4,dnz4]=toadomoi(cit(1),cit(2),cit(3),4,a,b,c);
    [dnx6,dny6,dnz6]=toadomoi(cit(1),cit(2),cit(3),6,a,b,c);
    [dnx7,dny7,dnz7]=toadomoi(cit(1),cit(2),cit(3),7,a,b,c);

    [a1]=diem_matphang(x(2),y(2),z(2),a,0,0,a,b,0,0,b,0);
    [a3]=diem_matphang(x(2),y(2),z(2),a,0,c,a,b,c,0,b,c);
    [a4]=diem_matphang(x(2),y(2),z(2),a,0,0,0,0,0,0,0,c);
    [a6]=diem_matphang(x(2),y(2),z(2),0,b,0,0,b,c,0,0,c);

[anr2]=diem_matphang(x(2),y(2),z(2),dnx3,dny3,dnz3,dnx7,dny7,dnz7,dnx6,dny6,dnz6);
[anr6]=diem_matphang(x(2),y(2),z(2),dnx7,dny7,dnz7,dnx6,dny6,dnz6,0,b,0);

[anf4]=diem_matphang(x(2),y(2),z(2),dnx1,dny1,dnz1,dnx4,dny4,dnz4,a,0,c);
[anf5]=diem_matphang(x(2),y(2),z(2),dnx1,dny1,dnz1,dnx2,dny2,dnz2,dnx3,dny3,dnz3);
```

```
        if (0<a1)&(0>a3)&(0<a4)&(0<a6)&(0<anr2)&(0>anr6)&(0>anf4)&(0>anf5) dk=1; else
dk=0; end


    case 12
        [vecint,xdirec,ydirec,zdirec]=vectorflexible(x1,y1,z1,x2,y2,z2,ti);
        cit=[vecint*xdirec;vecint*ydirec;vecint*zdirec];


        [dnx1,dny1,dnz1]=toadomoi(cit(1),cit(2),cit(3),1,a,b,c);
        [dnx2,dny2,dnz2]=toadomoi(cit(1),cit(2),cit(3),2,a,b,c);
        [dnx3,dny3,dnz3]=toadomoi(cit(1),cit(2),cit(3),3,a,b,c);
        [dnx7,dny7,dnz7]=toadomoi(cit(1),cit(2),cit(3),7,a,b,c);
        [dnx8,dny8,dnz8]=toadomoi(cit(1),cit(2),cit(3),8,a,b,c);


        [a1]=diem_matphang(x(2),y(2),z(2),a,0,0,a,b,0,0,b,0);
        [a2]=diem_matphang(x(2),y(2),z(2),a,b,0,a,b,c,0,b,c);
        [a4]=diem_matphang(x(2),y(2),z(2),a,0,0,0,0,0,0,0,c);
        [a6]=diem_matphang(x(2),y(2),z(2),0,b,0,0,b,c,0,0,c);



[anu3]=diem_matphang(x(2),y(2),z(2),dnx3,dny3,dnz3,dnx7,dny7,dnz7,dnx8,dny8,dnz8);
[anu6]=diem_matphang(x(2),y(2),z(2),dnx7,dny7,dnz7,dnx8,dny8,dnz8,0,0,c);

[anf1]=diem_matphang(x(2),y(2),z(2),dnx1,dny1,dnz1,dnx2,dny2,dnz2,a,b,0);
[anf5]=diem_matphang(x(2),y(2),z(2),dnx1,dny1,dnz1,dnx2,dny2,dnz2,dnx3,dny3,dnz3);


        if   (0<a1)&(0<a2)&(0<a4)&(0<a6)&(0>anu3)&(0<anu6)&(0<anf1)&(0>anf5)   dk=1;
else dk=0; end


    case 13
        [vecint,xdirec,ydirec,zdirec]=vectorflexible(x1,y1,z1,x2,y2,z2,ti);
```

```
cit=[vecint*xdirec;vecint*ydirec;vecint*zdirec];

[dnx1,dny1,dnz1]=toadomoi(cit(1),cit(2),cit(3),1,a,b,c)
[dnx2,dny2,dnz2]=toadomoi(cit(1),cit(2),cit(3),2,a,b,c);
[dnx3,dny3,dnz3]=toadomoi(cit(1),cit(2),cit(3),3,a,b,c);
[dnx4,dny4,dnz4]=toadomoi(cit(1),cit(2),cit(3),4,a,b,c);
[dnx5,dny5,dnz5]=toadomoi(cit(1),cit(2),cit(3),5,a,b,c);
[dnx6,dny6,dnz6]=toadomoi(cit(1),cit(2),cit(3),6,a,b,c);

[a2]=diem_matphang(x(2),y(2),z(2),a,b,0,a,b,c,0,b,c);
[a3]=diem_matphang(x(2),y(2),z(2),a,b,c,a,0,c,0,0,c);
[a4]=diem_matphang(x(2),y(2),z(2),a,0,0,0,0,0,0,0,c);
[a6]=diem_matphang(x(2),y(2),z(2),0,b,0,0,b,c,0,0,c);

[anf3]=diem_matphang(x(2),y(2),z(2),dnx3,dny3,dnz3,dnx4,dny4,dnz4,a,0,c);
[anf5]=diem_matphang(x(2),y(2),z(2),dnx1,dny1,dnz1,dnx2,dny2,dnz2,dnx3,dny3,dnz3);

[and1]=diem_matphang(x(2),y(2),z(2),dnx1,dny1,dnz1,dnx2,dny2,dnz2,dnx6,dny6,dnz6);
[and6]=diem_matphang(x(2),y(2),z(2),dnx5,dny5,dnz5,dnx6,dny6,dnz6,0,b,0);

    if  (0<a2)&(0<a3)&(0<a4)&(0<a6)&(0<anf3)&(0>anf5)&(0<and1)&(0<and6)   dk=1;
else dk=0; end

  case 14
    [a1]=diem_matphang(x(2),y(2),z(2),a,0,0,a,b,0,0,b,0);
    [a2]=diem_matphang(x(2),y(2),z(2),a,b,c,a,b,0,0,b,0);
    [a3]=diem_matphang(x(2),y(2),z(2),a,0,c,a,b,c,0,b,c);
    [a4]=diem_matphang(x(2),y(2),z(2),a,0,0,0,0,0,0,0,c);
    [a5]=diem_matphang(x(2),y(2),z(2),a,0,c,a,b,0,a,b,c);
    [a6]=diem_matphang(x(2),y(2),z(2),0,b,0,0,b,c,0,0,c);
```

```
    if (0<a1)&(0>a2)&(0>a3)&(0<a4)&(0>a5)&(0<a6) dk=1; else dk=0; end

end

%  Make decision

if (dk==0) disp('the inspected point is NOT INSIDE the flexible interdiction zone');
elseif (dk==1) disp('the inspected point is INSIDE the flexible interdiction zone');
end

stop=dk;
```

BIBLIOGRAPHY

[1]   A.D. Ngo, Y. Beauchamp, P. Le-Huy, S.N. Sean, and C. Kauffmann, 1997. "La sécurité dans l'utilisation de machine dangereuse : Les presses-plieuse dans le secteur de la fabrication d'équipement de transport et de machines," *Rapport de recherche ISST*.

[2]   CSST, 1985. "Dispositifs de protection sur les machines".

[3]   F. Beauchemin and S. Guertin, 1989. "Presses, cisailles, plieuses, étude des accidents dans cinq usines de fabrication de produits en métal," *Ergo norme Inc.*

[4]   P.A. Dressing and D.N. Valvano, 1997. "Control system for a hydraulic press brake," *United States patent number 5622915.*

[5]   N. Ariji and Kanagawa, 2005. "Device and method for controlling stop of hydraulic press and device and method for detecting trouble of speed selector valve," *United States patent number 6920821.*

[6]   R.M. Appleyyard and K.S. Davies, 2001. "Optical safety device for mounting on a moving member," *United States patent number 6316763.*

[7]   Sick, 2007. "V4000 Press Brake Sensor for safeguarding of press brakes", https://www.mysick.com/saqqara/get.aspx?id=IM0014597.

[8]   C. Kauffmann, P. Le-Huy, A.D. Ngo, and Y. Beauchamp, 1996. "A vision system with command by adaptive anticipation," in *International conference on human aspects of advanced manufacturing*, pp. 93-96.

[9]   J. Velten and A. Kummert, 2003. "FPGA-implementation of signal processing algorithm for video based industrial safety applications," *Lecture notes in computer science*, Springer Berlin, pp. 1004-1007.

[10]   Ik-Hwan Kim, Do-Eun Kim, You-Sung Cha, Kwang-hee Lee, and Tae-Yong Kuc, 2007. "An embodiment of stereo vision system for mobile robot for real-time measuring distance and object tracking," in *IEEE International conference on control, automation and system*, pp. 1029-1033.

[11]   Jong-Kyu Oh and Chan-Ho Lee, 2007. "Development of a stereo vision system for industrial robots," in *IEEE International conference on control, automation and system*, pp. 659-663.

[12]   T. Sogo, H. Ishiguro, and M.M. Trivedi, 2000. "Real-time target localization and tracking by N-ocular stereo," in *IEEE Workshop on omnidirectional vision*, pp. 153-160.

[13]   A.W. Fitzgibbon, M. Pilu, and R.B. Fisher, 1999. "Direct least squares fitting of ellipses," *IEEE Transactions on pattern analysis and machine intelligence*, vol. 21,pp. 476-480.

[14]   Radim Halir and Jan Flusser, 1998. "Numerically stable direct least squares fitting of ellipses," in *Proceedings of WSCG '98*, pp. 125-132.

[15]   P.L. Rosin, 1999. "Further five-point fit ellipse fitting," *Graphical models and image processing*, vol. 61, pp. 245-259.

[16]   J. Heikkila and O. Silven, 1997. "A Four-step Camera Calibration Procedure with Implicit Image Correction", in *IEEE Computer society conference on computer vision and pattern recognition*, pp. 1106-1112.

[17]   M.Z. Brown, D. Burschka, and G.D. Hager, 2003. "Advances in computational stereo", *IEEE Transactions on pattern analysis and machine intelligence*, vol. 25, pp. 993-1008.

[18]   L.G. Shapiro and G.C. Stockman, 2001. "Computer vision," *New Jersey: Pentrice Hall*, pp. 428-430.

[19]   www.stabilitytech.com/documents/CalculateSafetyDistances.doc

[20]   J.A. Janet, R.C. Lou, and M.G. Kay, 1994. "T-vectors make autonomous mobile robot motion planning an self-referencing more efficient," in *IEEE International conference on intelligent robots and systems*, pp. 578-594.

[21]   Videre Design, 2007. "STH-MDCS3/-C Stereo head user manual".

[22]   F. Noo, R. Clackdoyle, and C. Mennessier, 2000. "Analysis method based on identification of ellipse parameters for scanner calibration in cone-beam tomography," *Physics and medicine and biology*, vol. 45, pp. 3489-3508.